June 2020

Estimating the Onset and Extent of Dieback Of Phragmites australis Using the Normalized Difference Vegetation Index and Remotely Sensed Land Cover Classifications

Aimee M. Beaudette
Louisiana State University and Agricultural and Mechanical College

ESTIMATING THE ONSET AND EXTENT OF DIEBACK OF PHRAGMITES AUSTRALIS USING THE NORMALIZED DIFFERENCE VEGETATION INDEX AND REMOTELY SENSED LAND COVER CLASSIFICATIONS

A Thesis

Submitted to the Graduate Faculty of the
Louisiana State University and
Agricultural and Mechanical College
in partial fulfillment of the
requirements for the degree of
Master of Science

in

The School of Renewable Natural Resources

by
Aimee Margaret Beaudette
B.S., Rensselaer Polytechnic Institute, 2015
August 2020

ACKNOWLEDGEMENTS

I wish to express my sincerest gratitude to Dr. Andy Nyman for taking me on as a graduate student and providing me the resources to succeed. He has also given me plenty of opportunities to explore and learn about coastal Louisiana. I would like to thank Brady Couvillion, without his remote sensing expertise and helpful guidance, this project would not have been realized. Thank you to the members of my committee, Dr. Ashley Long and Dr. Sammy King, for taking time in their busy schedules to advise me.

A huge note of appreciation for my lab mates, friends, and other fantastic people I have met on this journey. You have made my experiences here unforgettable.

I would also like to acknowledge the love and support of my family, especially my parents. Even from afar, they have encouraged me throughout my studies and fielded many trivial phone calls, giving frank and sincere advice. Lastly, I am grateful to Joule for her constant companionship during the writing process and reminding me that there is always time for a run, a sniff, and a little fun.

TABLE OF CONTENTS

ABSTRACT

Phragmites australis is cosmopolitan plant species with an invasive variety present throughout most of North America. In the Balize Delta, Louisiana, USA, *P. australis* plays an important role in combatting subsidence, maintaining navigation channels, and protecting interior fish and wildlife habitat from waves and storm surge. In 2016 a dieback of *P.* australis was reported by wetland managers, coinciding with the appearance of an invasive Asian scale insect (*Nipponaclerda biwakoensis*), though the specific cause is still unknown. Two previous efforts attempted to identify the onset of dieback conditions met with limited success. Using Landsat images from 1985 to 2019 we classified *P. australis*. That classification was ground-truthed with information from five helicopter surveys made between 1988 and 2013. *P. australis* was stable from 2010 until 2014 but then decreased in area in 2015 and decreased in NDVI from 2014 to 2016. Area of total marsh vegetation and *P. australis* varied in similar patterns from the 1980s until the 2000s; since then, they vary in different ways. I concluded that detectable dieback conditions in the area began as early as 2014 and started recovery post 2016. Spatial patterns of decline is consistent with multiple stressors inducing dieback conditions such as eutrophication, salinity, or water level.

CHAPTER 1. INTRODUCTION

1.1. Global wetlands

Globally, wetlands cover between $2.0x10^{12}m^2$ and $6.7x10^{12}m^2$ of land (Matthews & Fung, 1987) and are valuable transitional ecosystems between open water and upland areas. They provide direct and indirect ecosystem services to adjacent areas and contribute to water quality, flood control, maintenance of biodiversity, production of consumer materials, recreational activities, and others (Keddy et al., 2009). The ecosystem services provided by wetlands have been valued up to \$14M per km^2 a year (Costanza et al., 2014).

Despite their economic and ecologic importance, we have experienced a global loss of wetlands area estimated up to 50% in the last century (McLeod et al., 2011). Coastal Louisiana itself lost approximately 4,870 km^2 of wetlands between 1932 and 2010(Couvillion et al., 2011). Furthermore, estimates suggest that an additional 4,500 km^2 are at risk of conversion to other land types or open water in the next 50 years, which may result in yearly costs between \$2.4 billion and \$23 billion from increased flooding (CPRA, 2012). A number of factors influence land loss, including construction of flood control levees, canal construction, decline of suspended sediments, wave erosion, subsidence, sea-level rise, and saltwater intrusion (Boesch et al., 1994).

1.2. The Balize Delta

River deltas are particularly important for fisheries, coastline defense, and economic centers while facing anthropological threats from these same uses. River deltas follow a cyclic pattern of regressive building and transgressive degradation. For example, the Mississippi River required 1,200 to 1,700 years to construct each lobe of its six delta lobes (Coleman et al., 1998).

The portion of a river delta that discharges water year-round and carries sediment is called active. Inactive portions discharge water only during flood seasons because sediment and vegetation obstruct flow during periods of low flow. Unlike active portions that generally build land, inactive portions enter a period of degradation. Even considering this cycle, wetland loss in major world deltas from agricultural and industrial use has been greater than losses from natural causes (Coleman et al., 2008).

The active delta of the Mississippi River occurs in two disconnected lobes (Coleman, 1988). The Atchafalaya delta is the newest actively building diversion, the Old River Control Structure, installed in 1963, prevents the Mississippi River from changing course to the newer lobe (Coleman et al., 1998). The older active lobe began its seaward advance between 800 and 1,000 years ago (Coleman, 1988). It is known as either the Birdfoot or Balize Delta; hereafter I will refer to this area as the Balize Delta (Coleman, 1988). The Balize Delta experienced wetland growth via six sub-delta lobes from the mid-1800s to the 1930s, it was then stable for many decades before entering a period of decline(Figure 1.) (Russell, 1967; Wells &Coleman, 1987). The Balize Delta has experienced at least three periods of such wetland creation and degradation as indicated by bay fill and peat deposits in the upper 10-m (Coleman, 1981). From 1932 to 2010, this area has seen persistent land loss of about 332 km^2 (Couvillion et al., 2011).

The Balize Delta contains important habitat for wildlife, provides protection to infrastructure, and serves as the entrance to major U.S. commerce ports. The shallow marine environments within the Balize Delta support coastal wildlife and fisheries. Within the Balize Delta are the Pass-a-Loutre Wildlife Management Area and the Delta National Wildlife Refuge, which together contain about 460 km^2 of wetland habitats protected from development.

Shipping ports in South Louisiana handle about 20% of waterborne commerce within the U.S. (Blum & Roberts, 2012). Of the four major shipping channels within the Balize Delta, Southwest Pass is the largest and most heavily managed by levees and dredging. In 2018, the U.S. Army Corps of Engineers, with the Louisiana Department of Transportation and Development, proposed a project to deepen the lower Mississippi River to 15 m, a project that would cost between $82–85 million initial investment and an average annual cost of $3-140 million (USACE, 2018). Changes in sedimentation within navigation channels would also impact management costs.

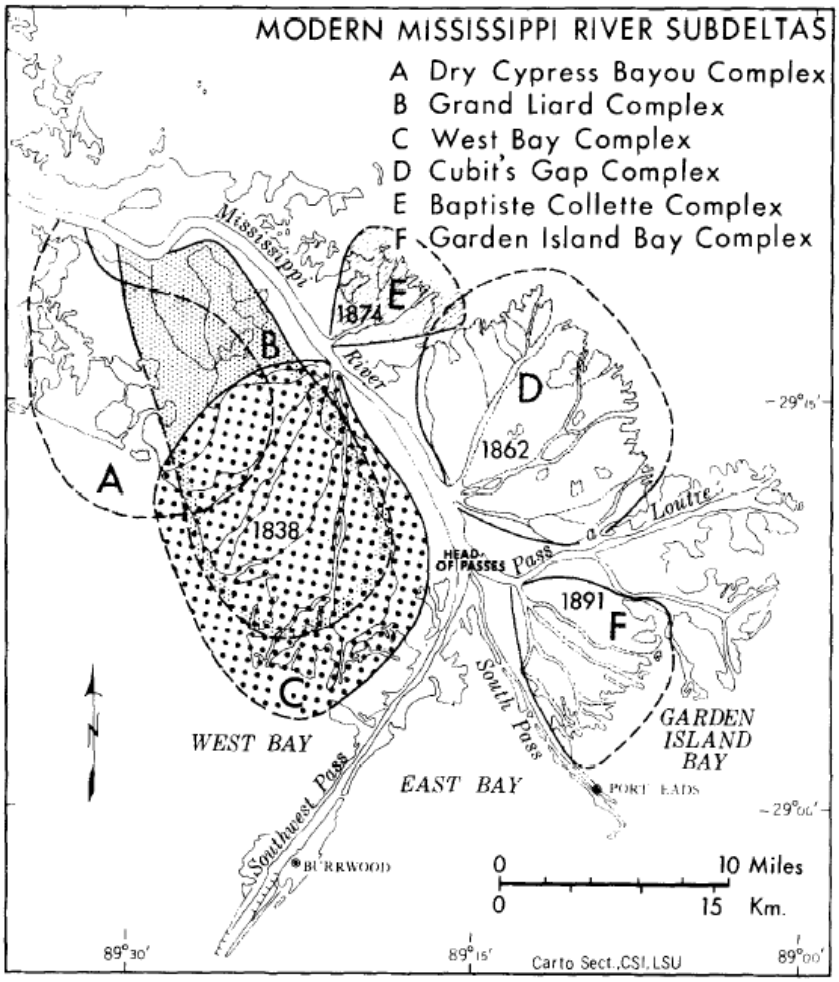

Figure 1. Map of the Balize Delta, Louisiana, USA showing the subdeltas and the dates of the crevasse openings. From Wells & Coleman (1987).

For coastal areas to survive and continue providing ecosystem services, their surface elevation change must match or exceed local relative sea level rise, maintaining an elevation that supports vegetation. In the Balize Delta, relative sea-level rise is about 1 cm/year due in part to geological subsidence, compared to 1.5 mm/year of global eustatic sea-level rise (Day et al., 2007). In Gulf Coast tidal freshwater marshes, mineral accumulation rates are shown to have the biggest impact on accretion rates (Neubauer, 2008). Most of the mineral sediment in the Balize Delta is introduced directly from riverine input (Coleman et al., 1998). Levees, used to reduce dredging costs by concentrating flow within the navigation channel, focus mineral sediments out the end of the river and reduce the input of riverine sediments into adjacent wetland environments, thus decreasing their accretion due to mineral inputs. Plant root growth and leaf litter can also contribute to accretion through organic soils (Cahoon et al., 1995). With reduced sediment inputs, the role of plants in organic accretion becomes increasingly important, especially in the inactive portions of the delta.

Other than non-technical descriptions by early European travelers such as one by E. Dekert in the mid-1880s who reported that the Balize delta was "reedy" (Trautmann, 1984), and mid-19th century drawings that appear to show *Phragmites australis*, vegetation in the Balize Delta was first described by Lloyd and Tracy (1901). At that time, much of the wetlands eventually created by the crevasses of the mid-1800s had not yet been created. They reported that the "passes" of the Mississippi River supported two associations: one being *P. australis* and the other being *Vigna* spp. and *Spartina* spp. Lloyd and Tracy (1901) excluded *P. australis* from their list of exotic plant species associated with ballast dumping, which suggests that *P. australis* in the Balize Delta was considered native, as do early writings and drawings.

O'Neil (1949), who prepared the first coastwide map of plant communities in Louisiana, also described and mapped vegetation in the Balize Delta. O'Neil reported that vegetation differed among new natural levees (e.g., *Typha latifolia, Zizaniopsis miliacea, and P. australis*), older more subsided natural levees (e.g., *S. alterniflora, Typha* spp., and *P. australis*), and extensive mud flats (e.g., *Scirpus americanus, Sagittaria platyphylla,* and *P. australis*). Like, Lloyd and Tracy (1901), O'Neil noted the presence of exotic species such as *Alternantherea philoxeroides* and *Eichornia crassipies* but did not include *P. australis* as exotic. Leatherman (1970) reported extensive floating marshes that probably formed as the recently deposited sediments continued to subside. Chabreck and Palimisano (1973) described vegetation before and after Hurricane Camille in 1972. They reported that *P. australis* and *S. alterniflora* were only slightly reduced by the hurricane, that *A. philoxeroides, Panicum repens* were greatly reduced by the storm, and that *A. philoxeroides* recovered significantly within one year. Vegetation maps prepared by Chabreck and Linscombe (1978, 1988, 1997) and Sasser et al. (2013) show gradual declines in fresh marshes in the Balize Delta as wetlands either converted to intermediate marshes or open water.

1.3. *Phragmites australis*

P. australis (Cav.) Trin. ex Steud., the dominant vegetation within the Balize Delta, is an aggressive cosmopolitan species that is studied globally, both within and outside of its native ranges (Hauber et al., 2011; Uddin et al., 2012). *P. australis* is known by a variety of names, including common reed, common cane, wild cane, reed grass, and more; in Louisiana it is commonly referred to as Roseau cane. The precise native range of *P. australis* is uncertain, but it is considered native or naturalized to large parts of the world (Plut et al., 2011). Pre-

Columbian aged *P. australis* has been found in sediments and archeological sites across North America (Kiviat & Hamilton, 2001). The oldest record of *P. australis* in North America dates to 40,000 to 11,000 years ago, recovered from sites of the extinct Shasta ground sloth, *Nothrotheriops shastense* Sinclair (Hansen, 1978). The Yuma skipper, *Ochlodes yuma* (Edwards), a butterfly endemic to the southwestern United States, is almost entirely restricted to *P. australis* stands (Scott et al., 1977). In 1900, vegetative surveys of the Balize Delta noted *P. australis* as native and the dominant species in the low-lying regions, further indicating the presence and importance of *P. australis* in the area (Lloyd & Tracy, 1901).

Though *P. australis* is one species, it can be classified into three main phenogeographic groups, North American, East Asian/ Australian, and European, with numerous distinct lineages within each group (Eller et al., 2017). *P. australis* is a perennial grass with long rhizomes and high growth rates (Lissner & Schierup, 1997). Patches of *P. australis* expand mostly through clonal expansion although seedling recruitment has also been documented (Kettenring et al., 2016). Recent spread of *P. australis* in North America has been attributed to the introduction of European genotypes (Marks et al., 1994). The introduction is believed to have occurred along the Atlantic coast and remained rare before 1910 but has since expanded across the continent (Saltonstall, 2002). Throughout North America, the introduced European variety is seen as a threat to native ecology and biodiversity (Marks et al., 1994). Introduced *P. australis* forms monospecific stands, replaces native marsh species of *Spartina* and *Juncus*, and alters soil nutrient pools (Able et al., 2003; Havens et al., 2003; Uddin & Robinson, 2017). This reduces plant diversity and can have negative effects on native estuarine species (Cook et al., 2018; Keller, 2000).

There are 11 haplotypes considered native to North America, however, these are not the haplotypes common in the Balize Delta (Table 1.) (Saltonstall, 2002). The Balize Delta is considered a hotspot of *Phragmites* diversity, with at least five distinct haplotypes identified by chloroplast DNA (Hauber et al., 2011; Lambertini et al., 2012). Haplotype I (Land-type), likely originating from Africa, is present but scarce within the Balize Delta, despite extensive distribution along the Gulf Coast, likely due to the absence of elevated habitats (Hauber et al., 2011; Pellegrin & Hauber, 1999; Saltonstall, 2002). The haplotypes AI and AD (collectively referred to as Greeny-type) are the rarest haplotypes in the Balize Delta, with similarities to samples from the Danube River Delta in Romania though its origin is undetermined (Lambertini et al., 2012). Haplotype M (European-type) is an intruder from Europe that has been reported as aggressively invasive across North America and is a minor component in the Balize Delta (Lambertini et al., 2012; Saltonstall, 2002). It may have arrived as late as the late 1900s or early 2000s. The dominant haplotype within the Balize Delta is M1 (Delta-type), which is distinguished from haplotype M and seems to have a native range in North Africa and the Mediterranean area (Hauber et al., 2011; Lambertini et al., 2012). The *P. australis* in the Balize Delta is all considered non-native (Kettering et al. 2012), though it predates the spread of the invasive European variety.

Table 1. Lineages, sublineages, haplotypes, and relative abundance of *Phragmites australis* in North America (adapted from Kettenring et al., 2012)

Lineage	Sublineage	Haplotypes	Approximate abundance in Balize Delta
Native *P. australis* subspecies *americanus*	None identified	A-H, S, Z, AA, AB, AC, E1, E2, E3, E4	Not present
P. australis subspecies *berlandieri* (Land, Gulf Coast Type)	None identified	I	Present but scarce
Introduced *P. australis*	Short B or EU	M	Scattered
	Short A or Greeny 1	M	Rare
	Delta	M1	Extensive
	Greeny 2	AD	Rare
	Greeny 3	AI	Rare

In the Balize Delta, *P. australis* plays an important role in buffering fragile habitats from salinity and waves, maintaining channelization of navigation channels, and buffering oil/gas infrastructure and recreational camps from storms (Suir et al., 2018). The loss of *P. australis* in the area will most likely result in increased costs from storm damage and navigational dredging. *P. australis* is a strong driver of accretion, collecting up to 70% more sediment than similar areas of *Spartina* species (Rooth & Stevenson, 2000). *P. australis* produces a lot of leaf litter and dried culms on the marsh surface, during erosive storms, this litter layer reduces the direct loss of sediments (Rooth et al., 2003). The ability of *P. australis* to trap and accumulate sediments could be important for long-term survival and marsh accretion. While *P. australis* collects sediments well, belowground productivity is the primary method by which *P. australis* increases surface elevation. A loss of *P. australis* in the Balize Delta could accelerate infilling of navigation channels with sediment as indicated by laboratory studies of the effects of vegetation on sedimentation in wetlands and associated tidal channels (Temmerman et al., 2012).

1.4. Dieback symptoms and scale infestation

During the fall of 2016, landowners and wetland managers reported that stands of *P. australis* were experiencing symptoms of dieback (Knight et al., 2018). Areas that were once dense stands of *P. australis* had thinned tremendously, some converted to open water, and leaves were browning earlier in the growing season.

P. australis dieback in the Balize Delta is assumed to be related to the infestation of *Nipponaclerda biwakoensis,* a non-native scale insect that was first identified in the area durring the summer of 2016 (Suir et al., 2018). Affected areas of *P. australis* in the Balize Delta had high population densities of *N. biwakoensis* in the fall of 2016, which represents the first record of infestation in the U.S. (Knight et al., 2018). The distribution of *N. biwakoensis* within Louisiana is primarily within the southeast parishes along the Mississippi River, though some infected plants have been recorded further west (Knight et al., 2018) and in southeastern Texas (Roseau Cane Die-Off: Distribution Map, 2019).

1.5. Research objectives

My first objective was to classify vegetation community types within the Balize Delta and to track changes in *P. australis* distribution through time. I also calculated the vegetation community types for subsections within the region to explore spatial variability in *P. australis* change over time.

My second objective was to determine if the dieback of *P. australis* in the Balize Delta could be detected using moderate resolution imagery. I used historic Landsat 5 and Landsat 8 images to identify *P. australis* and to detect changes in plant health and vigor using the normalized difference vegetation index (NDVI), which provides information on the greenness of

vegetation. I then isolated when the dieback of *P. australis* began to occur as well as whether it began uniformly across the region or localized.

I expected to see different patterns of dieback based on whether the dieback was primarily due to insect infestation or changes in environmental factors. If the primary cause of *P. australis* dieback was *N. biwakoensis* infestation, I expected that reduction in NDVI would start in a one or two localized areas of initial infestation and spread outward. Alternatively, if the main driver of dieback is an environmental or such as eutrophication, salinity, flood, or drought, I expected to observe a more concurrent, widespread decrease in NDVI across the study area.

CHAPTER 2. LITERATURE REVIEW

2.1. Marsh dieback

Marsh dieback is not a new phenomenon. A dieback event is characterized by a progressive decline in marsh vegetation beginning with thinning or browning of the aboveground foliage, which occurs during the regular growing season rather than winter senescence. Diebacks of *S. tonsendii* and *S. alterniflora* marshes have been well documented and mapped in Europe and North America (Goodman & Williams, 1961; Hughes et al., 2012; Marsh et al., 2016). Possible causes associated with recorded diebacks have been herbivores, nematodes, fungal pathogens, and abiotic stressors such as salinity, drought, or flooding (Elmer et al., 2013). The causes of other marsh dieback events in various wetland species have been attributed to eutrophication, accumulation of phytotoxins, and high water tables, as well as aphid and fungal infestation (Armstrong, Afreen-Zobayed, et al., 1996; Armstrong, Armstrong, et al., 1996; Mcdonald, 1955; van der Putten, 1997). In most cases, wetland ecologists suspect the role of multiple stressors on dieback conditions. Most previous dieback scenarios were followed by regrowth or recovery within a few years.

Dieback of *P. australis* has also been documented within Europe and Asia. Eutrophication (van der Putten, 1997), herbivory (Vermaat et al., 2016), winter flooding (Mcdonald, 1955), and phytotoxins (Armstrong & Armstrong, 2001) have been reported as potential causes of dieback in Europe. A non-native scale insect, *N. biwakoensis* is possible cause for the onset of *P. australis* dieback symptoms noted in the Balize Delta (Knight et al., 2018).

P. australis research in coastal North America has focused on its ability to replace Spartina spp. in coastal marshes of the Atlantic Coast of the United States (Bart et al. 2006). The dieback of *P. australis* in the Balize Delta appears to be the first report of a dieback of coastal *P. australis* but the coast of the Balize Delta is unlike the *Spartina* spp. marshes of the Atlantic coast. The Balize Delta has daily tides of ~0.6 m, which is about twice that elsewhere in coastal Louisiana but the tremendous discharge from the Mississippi River rarely allows salinity of surface waters to exceed 3 ppt (data from CRMS station 0153; see https://lacoast.gov/crms_viewer/Map/CRMSViewer). The *P. australis* dieback in the Balize Delta also appears different from previously reported *Spartina* spp. diebacks in that recovery of *Spartina* spp. often required years but once restablished, diebacks rarely returned. The dieback of *P. australis* in the Balize delta is characterized by two or even three dieback events within a single growing season and has been occurring every growing season since at least 2016. Furthermore, dieback does not affect all the *P. australis* simultaneously; patches a hundred or more hectares in dieback can be adjacent to equally large healthy patches.

2.2. Remote sensing and vegetation indices

Historically, field assessments have been used to measure and monitor conditions and infestations within coastal wetlands (Cardoch et al., 2002). *In situ* measurements over large geographic expanses can be expensive, time consuming, and impractical. Remote sensing techniques provide tools that can be used to detect, quantify, and monitor changes in coastal ecosystems over a variety of temporal, spatial, and spectral scales. Multiple vegetation indices have been developed for use in remote sensing to extract quantitative information on vegetation.

Vegetation indices are designed to provide information on vegetation greenness based on relative reflectance and absorption within specific electromagnetic bands. Because of chlorophyll in the leaves, vegetation absorbs energy in the red (0.6-0.7 μm) region of the electromagnetic spectrum while reflecting in the near infrared (NIR) (0.7-1.1 μm) (Chuvieco & Huete, 2010). A simple ratio of NIR to red reflectance is, however, sensitive to the soil beneath the canopy (Major et al., 1990). A variation of this simple ratio, the normalized difference vegetation index (NDVI) uses a non-linear transformation (Tucker, 1979). This transformation reduces the effect of extraneous noise and resulting in an index that is sensitive to low vegetation amounts (grasslands, semiarid, and arid environments).

NDVI provides an index that has a near-linear relationship to net primary productivity (Goward et al., 1985). As vegetation undergoes stress, its reflectance in the NIR decreases while reflectance in the red increases because of lower chlorophyll absorption. A lower contrast in NIR and red reflectance, therefore low NDVI, could be a result of lower quantities of vegetation in the pixel or the pixel containing vegetation that is stressed. While other vegetation indices exist, none are perfect. NDVI is very sensitive for detection of early season vegetation and in areas with less than 80% cover (Jackson et al., 1983).

2.3. Previous efforts to identify onset and extent of *P. australis* dieback in the Balize Delta

Dieback conditions within the Balize Delta were reported landowners and managers in the fall of 2016. The distribution of *N. biwakoensis* within Louisiana is primarily within the southeast parishes along the Mississippi River, though some infected plants have been recorded further west (Knight et al., 2018) and in southeastern Texas (*Roseau Cane Die-Off:*

Distribution Map, 2019). Two remote sensing reports were released shortly after the scale insect was identified in attempt to identify the period of onset and the extent of the dieback.

Ramsey et al. (2017) used cloud free Landsat images from six dates between 2014 and 2017 to track changes in *P. australis* health. After calculating NDVI for each image, the change in NDVI from the earlier to the later date of each pair was calculated. These change images were colored based on percent increase or decrease in NDVI and analyzed qualitatively. They showed a decrease in NDVI between July 2015 and April 2016 with a subsequent recovery by September 2016. While this method allows an easy visualization of change between images, it does not capture the long-term patterns and how these changes are deviations from historic cycles. Furthermore, the changes between images may be related to differences in conditions for that growing season rather than disturbance. Three of their dates were from 2016 and one of them the one in their data set from the end of a growing season. The lowest NDVI values thus might result from seasonal senescence or from dieback. In addition, Ramsey et al. (2017) assumed the dieback began after 2014, they looked at no earlier data. Last, there was no distinction among vegetation types, therefore they could have included salt marsh communities on the edges of the delta and different fresh marsh vegetation present at higher elevations

Suir et al. (2018) released a preliminary report using NDVI derived from Landsat images. They charted the mean NDVI in the Balize Delta from 2008 to 2017 with mixed interpretations of three distinct periods. From 2008 to 2011 the fluctuations were attributed to hurricanes followed by a ‘stable’ period from 2011 to 2015. The interpretation of a ‘stable’ period may be skewed by a lack of imagery in 2012 and 2013. From 2015 to 2017, there were fluctuations in mean NDVI attributed to dieback. The variation in NDVI attributed to hurricanes was much

wider than that attributed to dieback. For these basin wide NDVI calculations, there was no distinction among vegetation types, thus they could have included salt marsh communities on the edges of the delta and different fresh marsh vegetation present at higher elevations.

CHAPTER 3. DATA AND METHODS

3.1. Approach

I used a marsh vegetation type classification scheme to separate *P. australis* from other vegetation types. Dieback symptoms include thinning of *P. australis* stands and browning of standing stems during the growing season. To detect differences from average, I established baseline NDVI values within areas of *P. australis*. By comparing imagery seasonally, I minimize the effects of phonological cycles and other seasonal variations, thus, isolating the effects of dieback symptoms. I used Google Earth Engine, an online, server-sided computer program to process all satellite imagery.

3.2. Study area

Based on *N. biwakoensis* distribution, dominance of *P. australis,* and reports of dieback symptoms, I used a study area with approximately 2,108 km^2 of land and water of the Mississippi River Delta Basin with boundaries consistent with the Louisiana Coastal Area trend assessment boundary (Figure 2.). This subtropical region, centered at approximately 29.1^oN, -89.2^oW, contains mostly freshwater marshes and some fringing brackish and saline marshes.

I divided the region into subwatersheds as defined by the United States Department of Agriculture-Natural Resources Conservation Service, the United States Geological Survey (USGS), and the Environmental Protection Agency to aid in calculations by providing logical boundaries to divide the large geographic area (USGS & USDA-NRCS, 2013). The term subwatershed in this hierarchical classification is a misnomer and does not indicate that each is a true topographic watershed, but are instead a national dataset of polygons of comparable size that can be used (Omernik et al., 2017). The subwatersheds are identified by unique

hydrologic unit codes (HUCs) consisting of twelve digits. Hereafter, we will refer to the subwatersheds collectively by the term HUC12 to indicate level (code length) and individually by their names.

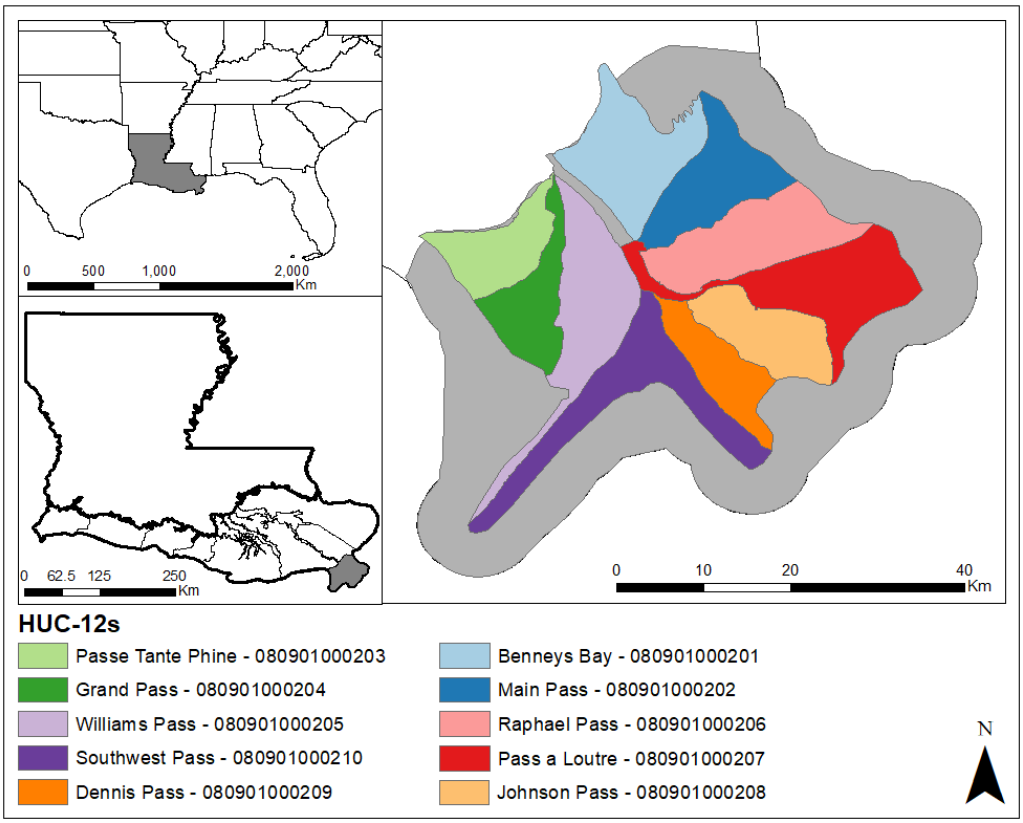

Figure 2. Location map for the study area, showing boundaries of the Mississippi River Delta Basin (Balize Delta) and the ten United States Department of Agriculture-Natural Resources Conservation Service twelve-digit code for subwatersheds within the region

3.3. Imagery and data

I used extended observational periods to account for historical variation and account for vegetation changes throughout the growing season. The use of multi-temporal data is increasing due to the increase in availability of remotely sensed data. The need for a long record of data and a frequent revisit time required me to use the Landsat satellite series for my analyses.

The Landsat program, jointly run by the National Aeronautics and Space Administration (NASA) and the USGS, is the only program of Earth Observing Satellites that has a virtually continuous record of more than 40 years. Satellites with higher spatial resolution or more frequent revisits, such as the WorldView series from DigitalGlobe, Inc. and the Sentinel series from the European Space Agency, lack the length of recording period that Landsat provides. Since 2008, the Landsat data archive has been open to the scientific community at no cost (Woodcock, 2008). The four sensors used in the Landsat family of satellites included (a) Landsats 1-3 Multi-Spectral Scanner (MSS) (1973-79), (b) Landsats 4-5 Thematic Mapper (TM) (1983-2012), (c) Landsat 7 Enhanced Thematic Mapper (ETM+) (1999-2012), and (d) Landsat 8 Operational Land Imager (OLI) (2013-present). Landsat MSS imagery, in its native spatial resolution, is coarser than the 30m resolution of Landsats 4-8, therefore I did not use this imagery to ensure consistent spatial resolution. In 1993, Landsat 6 was launched but failed to make it to orbit. Landsat 7 experienced instrument failure, resulting in missing data, I also excluded this sensor from analysis. Given these constraints, I used Landsat 5 and Landsat 8 imagery to cover my study period.

I used imagery collected between 1985 and 2019 in different combinations for each step or method. I used imagery from a three-year period for dominant vegetation community type classification, centered on a specific year of classification between 1985 and 2017. Both 2012 and 2013 were excluded because of a lack of imagery. I filtered all images within the period of record for Landsat 5 and 8, 1985 to 2019 to remove seasonal variation in *P. australis*. Lastly, to estimate seasonal averages of NDVI, I created a baseline of all Landsat 8 images from 2013

through 2019 for each season and a composite for each season of individual years. For the seasonal baseline, I used only Landsat 8 images (2013 to 2019) to avoid changes in sensors.

3.4. Image pre-processing

3.4.1. Atmospheric corrections

Electromagnetic radiation (visible and non-visible light) from the sun passes through the atmosphere twice before reaching the sensor, once on its way to Earth and once on its way back up. The atmosphere is composed mostly of molecular nitrogen and oxygen, but also contains water vapor, ozone, carbon dioxide, and aerosols such as dust, soot, and ice crystals. These molecules can affect the wavelength, spectral distribution, intensity, and direction of both incoming and reflected radiation. Because the atmosphere has a higher density than the near vacuum of space, electromagnetic radiation interacts more with particles and slows as it passes through. As light enters Earth's atmosphere, light is refracted, changing its angle; the effect depends on the angle of incidence, wavelength of light, and atmospheric conditions such as temperature, atmospheric pressure, and relative humidity (Ciddor, 1996). Radiation is absorbed at different wavelengths by molecules such as water vapor, ozone, and carbon dioxide (Baranov & Lafferty, 2012; Bera et al., 2010; Houghton, 1979). One of the most important processes occurring within the atmosphere is scattering, particularly in the visible spectrum (Chavez et al., 1991). Longer wavelength red and green light are scattered less than short wavelength blue light. Raleigh scattering is a term used to describe the diffuse scattering of light by particles smaller than the wavelength of incoming light. Satellite images, therefore, must be preprocessed to adjust for these atmospheric affects.

The U.S.G.S. generates Top of Atmosphere Reflectance, Surface Reflectance, and Top of Atmosphere Brightness Temperature using the Landsat Ecosystem Disturbance Adaptive Processing System (LEDAPS) for Landsat 5 and Landsat 8 Surface Reflectance Code (LaSRC) for Landsat 8 products. Level-1, terrain corrected data are converted into top of atmosphere reflectance and brightness temperature using calibration coefficients from the metadata (Chander et al., 2009). The Second Simulation of a Satellite Signal in the Solar Spectrum (6S) model is then used, as in standard Moderate Resolution Imaging Spectroradiometer (MODIS) spectral reflectance processing, to generate lookup tables for atmospheric correction algorithm (Maiersperger et al., 2013). The 6S model enables accurate accounting of elevated targets, simulated satellite observations, and directionally dependent and diffusely reflecting surfaces; auxiliary data such as ozone, water vapor, and Aerosol Optical Thickness area are also included in the model to generate the Surface Reflectance products (EROS, 2019a, 2019b; Kotchenova et al., 2006). The procedure for generation of Landsat 8 Surface Reflectance products follows the same structure but uses an internal algorithm rather than the 6S model. Both the LEDAPS and LaSRC methods provide masks for clouds, adjacent clouds, and cloud shadows. I used the Surface Reflectance products, including the cloud masks, in the next processing step.

3.4.2. Cloud recognition and exclusion

Cloud cover is a pervasive and unavoidable feature of satellite image collection, particularly in humid subtropical regions such as Louisiana. Detection and removal of cloud contaminated pixels is a prerequisite to image analysis. I used the “pixel_qa” band provided with the Landsat Surface Reflectance products for recognizing and removing clouds. This method allows for the detection and removal of clouds on a per-pixel basis, allowing for use of

non-clouded portions of the same image. Zhu & Woodcock (2012) proposed a method called Fmask (Function of Mask) that uses spectral and spatial information in the Landsat data to identify clouds based on scene-based thresholds and to match cloud shadows based on geometry. This algorithm was reprogrammed to C (called CFmask) by the USGS Earth Resources Observation and Science Center in 2013, and distributed along with Landsat 5 and 8 Surface Reflectance products as the Quality Assessment (QA) band (Zhu, 2017). The "pixel_qa" band provides Cloud Confidence and Cloud Shadow flags used to filter cloud contaminated pixels. For Landsat 5 images, I excluded the "pixel_qa" band values of 1, 72, 136, 80, 112, 144, 176, 160, and 224 from each image (Table 2.). Values of 1, 328, 336, 352, 368, 392, 400, 416, 432, 480, 834, 836, 840, 848, 864, 880, 898, 900, 904, 912, 928, 944, 992, 1350, and 1352 in the "pixel_qa" band for Landsat 8 images were excluded (Table 3.).

Table 2. Landsat 5 Pixel Quality Assessment (pixel_qa) values index (adapted from Landsat 4-7 Surface Reflectance (LEDAPS) Product Guide)

Attribute	Pixel Values
Fill	1
Clear	66, 130
Water	68, 132
Cloud Shadow	72, 136
Snow/Ice	80, 112, 144, 176
Cloud	96, 112, 160, 176, 224
Low Confidence Cloud	66, 68, 72, 80, 96, 112
Medium Confidence Cloud	130, 132, 136, 144, 160, 176
High Confidence Cloud	224

Table 3. Landsat 8 Pixel Quality Assessment (pixel_qa) values index (adapted from Landsat 8 Surface Reflectance Code (LASRC) Product Guide)

Attribute	Pixel Values
Fill	1
Clear	322, 386, 834, 898, 1346
Water	324, 388, 836, 900, 1348
Cloud Shadow	328, 392, 840, 904, 1350
Snow/Ice	336, 368, 400, 432, 848, 880, 912, 944, 1352
Cloud	352, 368, 416, 432, 480, 864, 880, 928, 944, 992
Low confidence cloud	322, 324, 328, 336, 352, 368, 834, 836, 840, 848, 864, 880
Medium confidence cloud	386, 388, 392, 400, 416, 432, 898, 900, 904, 928, 944
High confidence cloud	480, 992
Low confidence cirrus	322, 324, 328, 336, 352, 368, 386, 388, 392, 400, 416, 432, 480
High confidence cirrus	834, 836, 840, 848, 864, 880, 898, 900, 904, 912, 928, 944, 992
Terrain occlusion	1346, 1348, 1350, 1352

The algorithms used for cloud recognition produce relatively cloud-free images, though some clouds remain. As such, I employed a compositing method to exclude anomalous values from median composites. Within a given season, I calculated a median value for each for each pixel. Seasonal composites for individual years include an average of seven images. If the majority of those seven images contained erroneous cloud recognition flags, it is possible that the effects could be present in these pixels of the potentially affected years.

3.4.3. Normalized Difference Vegetation Index

The NDVI, described previously, was calculated for each pixel of each image used and added as a separate band of data. The formula for NDVI is shown below (Equation 1.):

Equation 1. $$NDVI = \frac{\rho_{NIR} - \rho_{red}}{\rho_{NIR} + \rho_{red}}$$

The terms ρ_{NIR} and ρ_{red} indicate the reflectance of a pixel in the near infrared and red bands respectively. Reflectance values are unitless, as they represent the ratio of the amount of light leaving a target to the amount of light striking the target. NDVI has a range from -1 to +1.

Negative values are given by clouds, snow, water and ice while bare ground give values ranging from -0.1 and +0.1 (Goward et al., 1985). Values closer to +1.0 are given as the amount of green vegetation increases (Tucker, 1979). Because water has a lower NDVI value than vegetation, the presence of water within a pixel lowers the overall NDVI. Noise within data from clouds, water, and snow tend to decrease NDVI values, false high values are less common (Pettorelli et al., 2005). In future steps, using value compositing of seasonal image collections is a way to reduce some of these errors. I also used a linear mixing model to separate pixels that contain both land and water, described later.

3.4.4. Modified Normalized Difference Water Index

Indices also exist based on the reflective and absorptive properties of water. A band ratio approach similar to the NDVI can be used to identify water. A direct ratio can suppress land and vegetation signals while amplifying water signals, though it cannot remove the effects of land and vegetation. A normalized difference water index (NDWI) using a green band and a near infrared band was proposed to solve this problem (McFeeters, 1996). Using this approach, built up land and water can have similar signals as both features reflect green light more than near infrared (Xu, 2006). I used a modification of the NDWI (mNDWI), using the middle infrared (MIR) band to enhance the discrimination of water from non-water features (Equation 2.).

Equation 2.
$$mNDWI = \frac{\rho_{green} - \rho_{MIR}}{\rho_{green} + \rho_{MIR}}$$

The terms ρ_{MIR} and ρ_{green} represent the reflectance of a pixel in the MIR and green bands respectively. The mNDWI produces and index with values ranging from -1 to +1. Using this index, water will have positive values from higher absorption in the MIR band. Built up land reflects more in the MIR band than it does in the green band, having a negative value using this

index (Xu, 2006). Soil and vegetation will also have negative values based on their reflectance in the MIR band (Jensen, 2005). The mNDWI for each pixel was calculated for each pixel and added to each image as a band of data.

3.4.5. Floating aquatic vegetation correction

Generally, water and land are spectrally distinct based on their reflectance and absorbance in different bands, making separating the classes fairly easy. However, with floating aquatic vegetation, it can become a complex separation. Areas with floating vegetation have a strong vegetation signal, just as on land. Areas of water with floating aquatic vegetation may therefore be misidentified as land, instead of water. While aquatic vegetation has a strong vegetation signal, it also has some water signal that gets through; these signals vary as the vegetation moves within or on the surface. Using the changes of the NDVI and mNDWI indices of pixels through the period of record, areas of possible aquatic vegetation are identified and used as an aquatic vegetation mask. This mask was used with mNDWI endmembers for a Linear Spectral Unmixing method to estimate the fraction of each pixel that contains aquatic vegetation. Pixels with greater than 0.001 percent land were identified as land and used in further steps.

3.5. Vegetation type classification

To track the changes in vegetation health attributed only to *P. australis*, I classified images into land cover types and then into marsh vegetation community types. The vegetation community types chosen were based on a classification used to delineate vegetation community types in Louisiana using self-organizing maps and helicopter-based observational

data (Snedden, 2019). I classified a composite from each year between 1985 and 2017, excluding 2012 and 2013 due to the absence of available imagery.

3.5.1. National Land Cover Database type classification

Classification of vegetation community types occurred in several hierarchical steps. Using the methods described above, a collection of images from each year (1985-2017) were preprocessed, composited based on median values, and then separated into land and water categories. I then classified the land category into categories described in the National Land Cover Database (NLCD) (Table 4.) (Jin et al., 2019). The purpose of this second classification is to isolate the portions of the Balize Delta that are emergent herbaceous wetlands. The emergent herbaceous wetlands were further delineated into the vegetation community types (Table 5.) described in Snedden (2019).

Table 4. National Land Cover Database 2016 values and classifications

Value	Classification
11	Open water
22	Developed, low intensity
23	Developed, medium intensity
24	Developed, high intensity
31	Barren land
90	Woody wetlands
95	Emergent herbaceous wetlands

3.5.2. Harmonic analysis

Phenology deals with the timing of recurrent vegetation life cycle events, such as leaf growth, flowering, and senescence. A plant's phenology has influence on ecosystem dynamics, and vice versa, and determines interrelationships between different species (Butt et al., 2015). Various species often have differing seasonal cycles, reaching peak greenness and beginning senescence at characteristic times. To aid in classification of vegetation communities, these

basic annual temporal cycles can be characterized using harmonic analysis. Harmonic analysis, based on the Fourier transformation, uses superimposed sines and cosines to represent annual cycles of reflectance as a wave. The Fourier transformation has been applied to the temporal signature of time series vegetation images and shown to be sensitive to systematic changes (Moody & Johnson, 2001). Time series data contains both seasonal and abrupt changes; the processing of these temporal data help to show the characteristics of associated seasonal trends to separate disturbances from natural cycles (Jakubauskas et al., 2001; Roy & Yan, 2020). Using harmonic analysis, I calculated a seasonality wave for each pixel; each wave represents the intra-annual pattern of NDVI specific to that pixel.

I used harmonic analysis in the classification scheme to use seasonality as a variable in the classification algorithms. The collection of Landsat images was first filtered to an individual year (each year between 1985 and 2011) then corrected for atmospheric factors and cloud exclusion. NDVI and mNDWI indices were calculated as described above and added as new bands to each image. The median values of each band were calculated from this collection and used to delineate water and land as previously described. The land portion was used for National Land Cover Database type classification. For each year, a harmonic signal was calculated for each land pixel using all cloud-free values during a 3-year period of Landsat 5 imagery centered on the year of interest. This analysis tracks the seasonal pattern over a 3-year period because weather and conditions change over time. After addition of a time band, the sines and cosines were calculated. After a linear least squares regression, coefficients of the harmonic trend were used to compute fitted values of NDVI. The three values resulting from

the harmonic analysis represent the phase, amplitude, and mean NDVI value of a wave representing the values of that pixel for the three-year period.

3.5.3. Principal component analysis

I used principle component analysis (PCA) to account for the majority of variance present in the reflectance data. PCA is a statistical approach that uses linear transformations to convert a set of variables into a set of linearly uncorrelated variables called principal components; they are ordered by the amount of variance explained (Mather, 1987). The first two components have been used in land-cover classifications and explain over 90% of the variance (Townshend et al., 1985). PCA of NDVI time series provides a way of tracking responses of vegetated land surfaces (Hall-Beyer, 2003). The principal components are useful in uncovering significant changes over long periods of time and isolating anomalous events (Eastman & Fulk, 1993). The first component corresponds to the integrated vegetation index, resembling the average, and the second represents that seasonality of vegetation index values (Townshend et al., 1985).

The yearly median composites were used to compute the principal components, using bands 2, 3, 4, 5, 7, mNDWI, and NDVI. The covariance values of the bands were computed within the region and eigen analysis performed to separate the values and vectors. The principal components were normalized by their standard deviations and the first 3 components were added to the dataset.

3.5.4. Final NLCD classification

The classification of each yearly composite was completed using multiple iterations of a Classification and Regression Tree (CART) analysis. A CART classifier uses a decision tree to filter

data into separate classes based on binary splits (Breiman et al., 1984). The classifier is created using data with known classes and a set of independent variables. Independent variables used in our classifier included the median composites of bands 2, 3, 4, 5, 7, mNDWI, NDVI, the seasonality layer from harmonic analysis, and the first three principal components. A collection of National Land Cover Database images from 1992, 2001, 2004, 2006, 2008, 2011, 2013, and 2016 was created and the mode taken for each pixel, to be used as training data. A random selection of 200,000 pixels were selected from the National Land Cover Database mode as training points in the CART classifier. Five iterations of the CART classifier using different sets of random points were run with the mode taken as the final classification for each year. An error matrix and kappa value were calculated for each iteration of the CART classifier. The error matrix compares points classified by the algorithm to reference data provided, the National Land Cover Database. User and producer accuracy were calculated for each class. User accuracy represents how often the class given in the map is present on the ground and producer accuracy represents how often features on the ground are appropriately classified on the map. From these the overall accuracy of the classification is calculated. The Kappa statistic is a unit-less measurement of how the classification method preforms compared to randomly assigning values. Kappa can range from -1 to 1 with 0 indicating classification the same as random assigning, 1 significantly better than random assigning, and -1 significantly worse than random assigning. The area of each National Land Cover Database class (Table 4.) within the Balize Delta was calculated for each year between 1985 and 2011. Pixels classified as Emergent Herbaceous Marsh were masked and used for further classification in subsequent steps.

3.5.5. Marsh type classification

A second annual classification into the vegetation community types described in Snedden (2019) followed a similar method as the NLCD classification (Table 5.). A collection of images from each year (1985-2017) were atmospherically corrected, filtered for clouds, NDVI and mNDVI calculated, and composited based on median values of bands 2, 3, 4, 5, 7, NDVI, and mNDWI. The harmonic analysis and PCA were calculated as described for the NLCD classification. The seasonality from harmonic analysis of emergent herbaceous wetlands and three principal components were added to the median composite. A salinity score dataset was also added to the image stack, the salinity scores are based on dominant vegetation type (Visser et al., 1998). Four 'vegetative types' have been described for coastal Louisiana based on common plant compositions and associations (Chabreck, 1970). These vegetation types have been given rough salinity ranges they are thought to represent. For the dataset used, the coastal zone is broken into four vegetation-salinity zones: saline marsh (8-29 ppt), brackish marsh (4-18 ppt), intermediate marsh (2-8 ppt), and fresh marsh (0-3 ppt), each vegetation-salinity zone is represented by the middle of the range, 18 ppt, 10 ppt, 4 ppt, and 0 ppt respectively (Visser et al., 1998). Across the coastal zone, salinity can play an important role in predicting vegetation, but the salinity layer most likely did not affect the classification of the Balize Delta because it is almost entirely fresh marsh.

Table 5. Three most abundant taxa with percent mean relative error for each community type, adapted from Snedden, 2019

Community Type	Three most abundant taxa (mean % relative cover)
Maidencane	*Panicam hemitomon* (34%), *Leersia hexandria* (11%), *Sagittaria lancifolia* (10%)
Three-square	*Schoenoplectus americanus* (27%), *Spartina patens* (19%), *Sagittaria lancifolia* (6%)
Roseau Cane	*Phragmites australis* (71%), *Spartina patens* (5%), *Alternanthera philoxeroides* (4%)
Paspalum	*Paspalum vaginatum* (24%), *Schoenoplectus californicus* (13%), *Spartina Patens* (11%)
Wiregrass	*Spartina patens* (65%,) *Distichlis spicata* (7%), *Schoenoplactus americanus* (5%)
Bulltongue	*Sagittaria lancifolia* (16%), *Polygonum punctatum* (11%), *Alternanthera philoxeroides* (7%)
Needlerush	*Juncus roemerianus* (54%), *Spartina alterniflora* (15%), *Spartina patens* (8%)
Bulrush	*Bolboschoenus robustus* (24%), *Distichlis spicata* (16%), *Spartina patens* (13%)
Brackish Mix	*Spartina alterniflora* (53%), *Spartina patens* (20%), *Juncus roemerianus* (10%)
Oystergrass	*Spartina alterniflora* (93%), *Juncus roemerianus* (4%), Spartina *patens* (1%)
Saltgrass	*Distichlis spicata* (49%), *Spartina patens* (21%), *Spartina alterniflora* (15%)

After masking to emergent herbaceous marsh in each image, the images were classified using a series of 4 CART classifiers and 3 Random Forest classifiers using helicopter survey data as training data. The helicopter surveys have been conducted approximately every 10 years from 1968-2013; surveys from 1988, 1997, 2001, 2007, and 2013 were used in this classification and provide ground-truthing. The Random Forest classifier is a non-parametric classifier that uses an ensemble of CARTs to make a prediction (Breiman, 2001). Each CART classifier casts a single vote and the class with the maximum number of votes is selected as the classification. Random Forests have become popular in remote sensing due to the accuracy of land cover classification and ability to handle highly dimensional data (Belgiu & Drăgu, 2016; Rodriguez-Galiano et al., 2012). After classification, an error matrix and kappa value were calculated, as previously described, for each CART and Random Forest classifier. The areas of each vegetation community type within the Balize Delta and within individual HUC12s were calculated for each

year between 1985 and 2017. The *P. australis* dominated vegetation community was masked and used in subsequent steps.

3.6. Fitted NDVI through time

NDVI was charted through time within individual HUC12s to assess when the dieback may have begun. The collection of atmospherically corrected Landsat 5 and 8 Surface Reflectance imagery was first filtered to exclude May images for each year, due to complications with sun glint. Then, NDVI and mNDVI were calculated and added to the images. Cloud cover was calculated based on the "pixel_qa" described before and only images that contained 5% or less of clouds were used. For example, in Benney's Bay (HUC-080901000201), it was determined that 189 of 388 Landsat 5 images and 43 out of 108 Landsat 8 images were cloud free; those were the images used in the following calculations. As described previously, we calculated the harmonics of the time series, this time using the period of record from 1985 to 2019. The difference between observed NDVI values for each pixel and the values fitted from the harmonic analysis is the remainder that is not explained by normal seasonal variation and s centered on 0. These remainder values were plotted against time to see deviations of NDVI values from expected cycles in each HUC12.

A penalized regression smoothed spline was applied to the NDVI remainders in each HUC12. In this method, polynomial pieces, or splines, are joined at certain values of x, called the knots (Eilers & Marx, 1996). The number of knots used is an important decision, as too many can cause overfitting of the data whereas too few could cause underfitting, There is a minimum adequate value of the number of knots, using more than this value provides satisfactory fits (Ruppert, 2002). The use of penalization allows each spline to use a maximum

polynomial order without overfitting the model. For each HUC12, the number of knots used, essentially the effective degrees of freedom, and the r-squared values were calculated. The smoothed regression values and 95% confidence interval were plotted against time. A sum of the regression lines in each HUC12 was also plotted against time, to see a generalized trend.

3.7. Seasonal differences from average

To view and analyze the spatial extent of dieoff symptoms, we mapped the difference between average seasonal NDVIs from a baseline average. Baseline averages were calculated for each season and derived from the period of record for the Landsat 8 satellite, 2013 through 2019. A baseline of 2013 to 2019 was chosen to avoid any differences in scanners between Landsat 5 and 8 and to avoid anomalous hurricane years. The boundaries for the seasons were chosen based on seasonal dates in coastal Louisiana (Table 6.), there is some overlap in seasonal definitions to allow each season to have enough cloud free images. The winter seasons were defined as the November before to February of the year analyzed, for example winter of 2016 is November 2015 through February 2016. Landsat has a return period of 16 days, so having more than 100 days in each seasonal interval allows for more than 6 images per season each year, increasing the chances of cloud free imagery. After image pre-processing including atmospheric corrections, cloud exclusion, and the addition of NDVI and mNDWI, I created a baseline composite for each season based on the mean. For each season, after the same image pre-processing, a year specific composite was calculated using the mean. A difference from average image was calculated for each season and year from 2013-2019, by subtracting the baseline mean from the mean for the year and season of interest.

Table 6. Louisiana specific definitions of seasons with the average number of Landsat images collected in a year per season

Season	Beginning Date	Ending Date	Average # images per year
Winter	Nov-15th	Feb-28th	6.6
Spring	Feb-1st	June-25th	8.3
Summer	May-16th	Sept-30th	8.6
Fall	Sept-1st	Dec-18th	6.6

CHAPTER 4. RESULTS

4.1. Vegetation classification

Error matrices were calculated for each iteration of CART classifier for each year of NLCD classifications performed; our classification method resulted in a mean kappa value of 0.575 and an accuracy of 80% for 1985 (Table 7.). Producer accuracy for emergent herbaceous wetlands was 82%, meaning that 82% of herbaceous wetlands on the ground were appropriately classified on the map. A user accuracy of 89% is also a measure of reliability and means that 89% of areas classified as herbaceous wetlands are found on the ground. The NLCD type classification resulted in seven classes within the Balize Delta: open water (10%), barren land (<1%), woody wetlands (2%), emergent herbaceous wetlands (86%), and low (<1%), medium (<1%), and high (<1%) intensity developed land (Figure 3.). The amount of herbaceous marsh grew from 1985-1995 where it has remained fairly stable with around 380 km^2 of herbaceous wetlands each year save for a drop in 2005, assumed to be from Hurricane Katrina (Figure 4.).

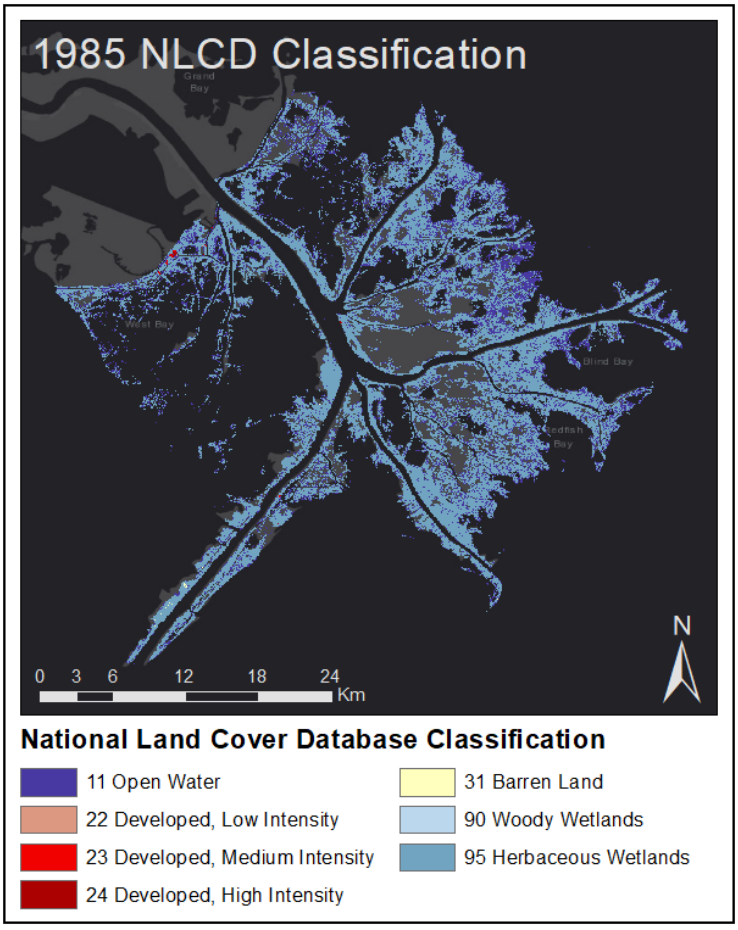

Figure 3. National Land Cover Database like classification for 1985 in the Balize Delta, Louisiana, USA

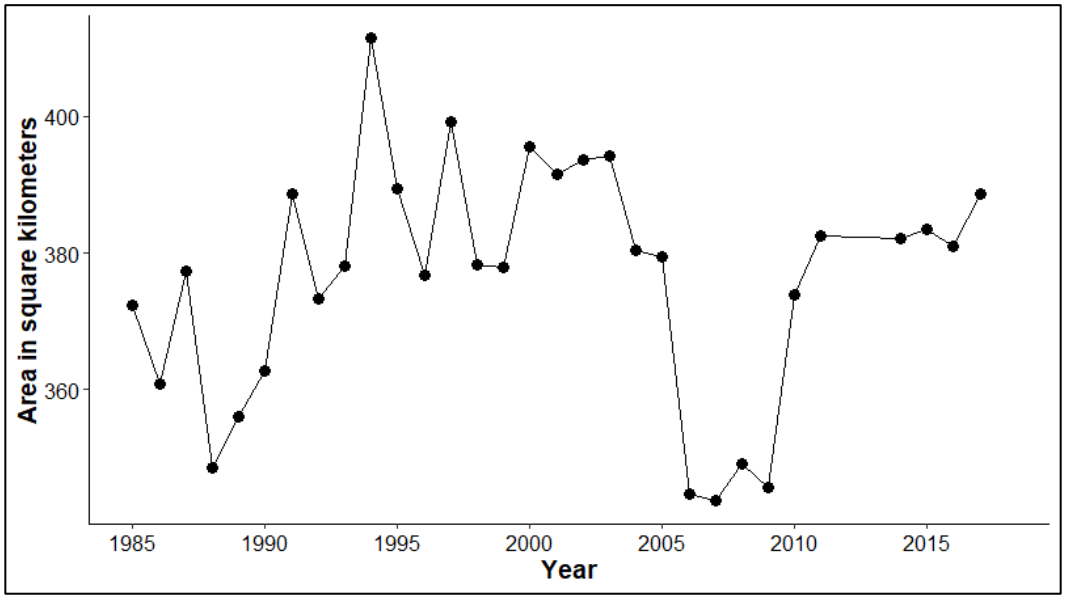

Figure 4. Area in square kilometers of National Land Cover Database emergent herbaceous wetland in the Balize Delta, Louisiana, USA from 1985 to 2017

Table 7. Error matrix of pixel counts for CART classifier from a remote sensing classification using Landsat 5 imagery for a National Land Cover Database type classification for 1985 in the Balize Delta, Louisiana, USA, with an overall kappa statistic of 0.5777

		National Land Cover Database Class								
		Open Water	Dev., Low	Dev., Med	Dev., High	Barren	Woody Wetland	Herbaceous	Total	User Accuracy
Predicted Class	Open Water	8642	1	1	0	21	2	3921	12588	0.6865
	Dev, Low	7	4	2	0	0	0	23	36	0.1111
	Dev, Med	2	3	14	1	1	0	11	32	0.4375
	Dev, High	6	0	2	11	0	0	7	26	0.4231
	Barren	113	0	0	0	36	0	283	432	0.0833
	Woody Wetland	14	0	0	0	0	32	91	137	0.2336
	Herbaceous	2417	3	4	1	21	19	20265	22730	0.8916
	Total	11212	11	23	13	79	53	24612	35981	
	Producer Accuracy	0.7708	0.3636	0.6087	0.8462	0.4557	0.6038	0.8234		Total: 0.8061

* Dev., Developed

Each year that vegetation community type classifications were run, error matrices were calculated for each iteration of CART classifier as well as each Random Forest classifier (Table 8.). The average kappa value for the CART and Random Forest classifiers used in the 1985 vegetation community type classification were 0.64 and 0.75 respectively, with average overall accuracies of 0.69 and 0.79. Producer accuracy for *P. australis* was 45% and user accuracy was 75%. Hence, 45% of *P. australis* on the ground was appropriately classified on the map and that 75% of *P. australis* areas on the map were present on the ground.

Vegetation community type classification resulted in the presence of all 11 marsh vegetation community types described in Snedden (2019) (Table 5.) within the Balize Delta, which included Roseau cane (296 km^2), wiregrass (25 km^2), bulltongue (10 km^2), three-square (10 km^2), bulrush (4 km^2), saltgrass (3 km^2), maidencane (2km^2), oystergrass (2 km^2), needlerush (<1 km^2), and brackish mix (<1 km^2) (Figure 5a.). Between 1985 and 2017, the majority of the Balize Delta has been classified as *P. australis* for many of the years, excepting on levees along Southwest Pass and the main channels of the River (Figure 5b.) The area of all vegetation community types calculated for each image have fluctuations in area with a noticeable drop in 2005 that persisted for several years, most likely because of Hurricane Katrina (Figure 6a.). The area of *P. australis*, did not decline in 2005, but instead slowly declined between 2008 and 2015 with a rebound in 2016 and 2017 (Figure 6a.). The areas of vegetation community types other than *P. australis* remained at similarly low levels throughout the time period with notable increases of needlerush, paspalum, and wiregrass after 2010 (Figure 6b.). Surprisingly, increases in needlerush and wiregrass appear common in all HUC12s even though those types are common only at the northern ends of the Balize Delta where riverine inputs are slight.

Vegetation community types were further divided into areas within individual HUC12s (Figure 7.). In Passe Tante Phine, Grand Pass, Williams Pass, Southwest Pass, and Benney's Bay, the area of total vegetation has an increasing trend through 2017. Total vegetation in Pass a Loutre, Johnson Pass, and Dennis Pass is decreasing in area. Lastly, the total vegetation area in Raphael Pass and Main Pass appear to hold steady throughout the period of analysis.

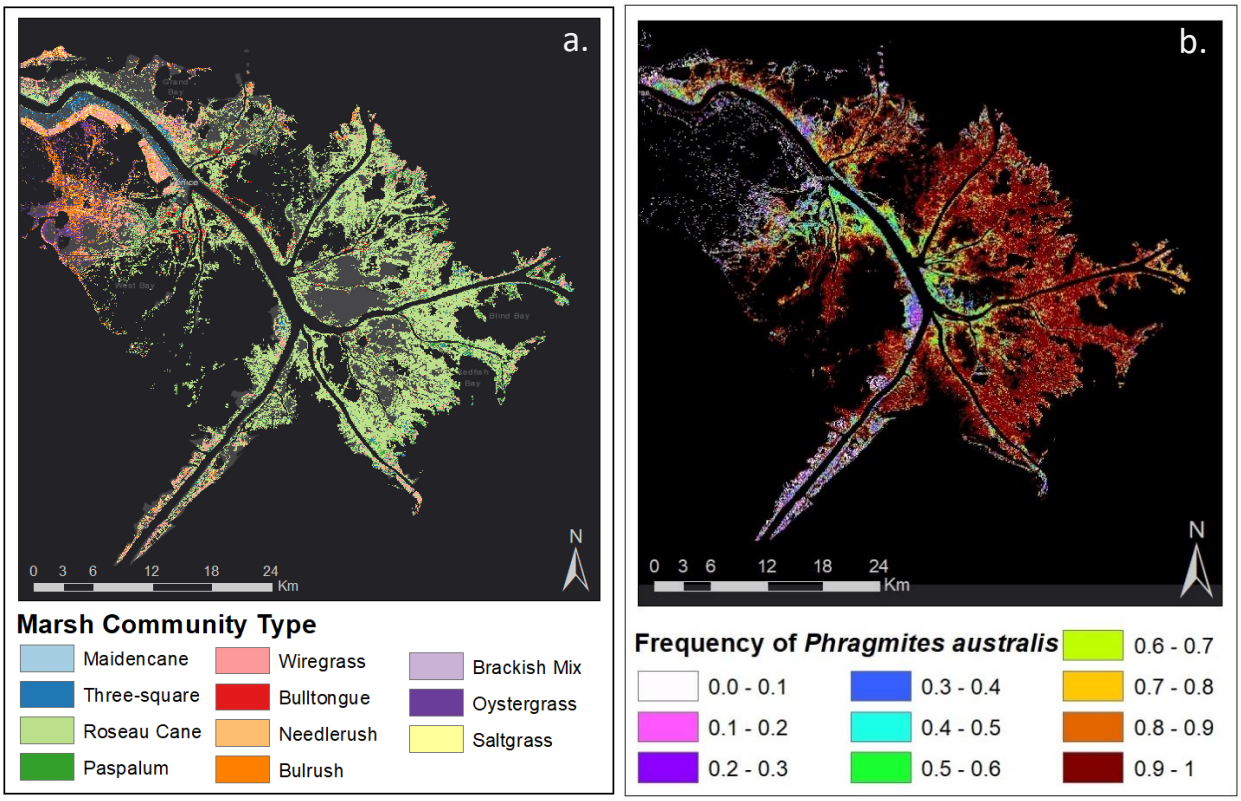

Figure 5. Vegetation maps in the Balize Delta, Louisiana, USA (a). Marsh vegetation community type classification for 1985 (b). Frequency that each pixel was classified as *Phragmites australis* between 1985 and 2017

Table 8. Error matrix for one iteration of CART classifier used in the classification of marsh community type for 1985 in the Balize Delta, Louisiana, USA, with pixel counts for classification of marsh community type, user and producer accuracy, and an overall kappa statistic of 0.634

		Actual class*												
		Maid.	Three	Roseau	Pasp.	Wire.	Bull.	Needle.	Bulrush	Brackish	Oyster.	Salt.	Total	User Accuracy
Predicted Class	Maid.	15782	1406	463	580	98	3732	0	0	2	1	19	22083	0.7147
	Three	1092	10174	1546	3412	1934	659	7	7	1	0	111	18943	0.5371
	Roseau	23	645	6150	722	120	275	14	30	1	21	175	8176	0.7522
	Pasp.	183	3601	1695	12114	2991	1900	2	5	0	1	113	22605	0.5359
	Wire.	42	6098	2278	7625	71395	170	1077	1397	312	122	2737	93253	0.7656
	Bull.	4070	2263	1253	1971	95	30990	2	5	0	4	113	40766	0.7602
	Needle.	0	16	3	25	125	0	2042	1360	1220	478	121	5390	0.3788
	Bulrush	0	47	49	113	259	0	1628	3989	1673	724	602	9084	0.4391
	Brackish	0	44	8	66	378	1	860	1288	2053	371	126	5195	0.3952
	Oyster.	0	43	78	61	11	0	1429	1343	1190	20947	368	25470	0.8224
	Salt.	3	148	229	203	611	41	168	334	81	197	2156	4171	0.5169
	Total	21195	24485	13752	26892	78017	37768	7229	9758	6533	22866	6641	255136	
	Producer Accuracy	0.7446	0.4155	0.4472	0.4505	0.9151	0.8205	0.2825	0.4088	0.3143	0.9161	0.3246		Total: 0.6969

*Maid., maidencane; Three, three-square; Roseau, Roseau cane; Pasp., paspalum; Wire., wiregrass; Bull., bulltongue Needle., needlerush; Brackish, brackish mix; Oyster., oystergrass; Salt., saltgrass

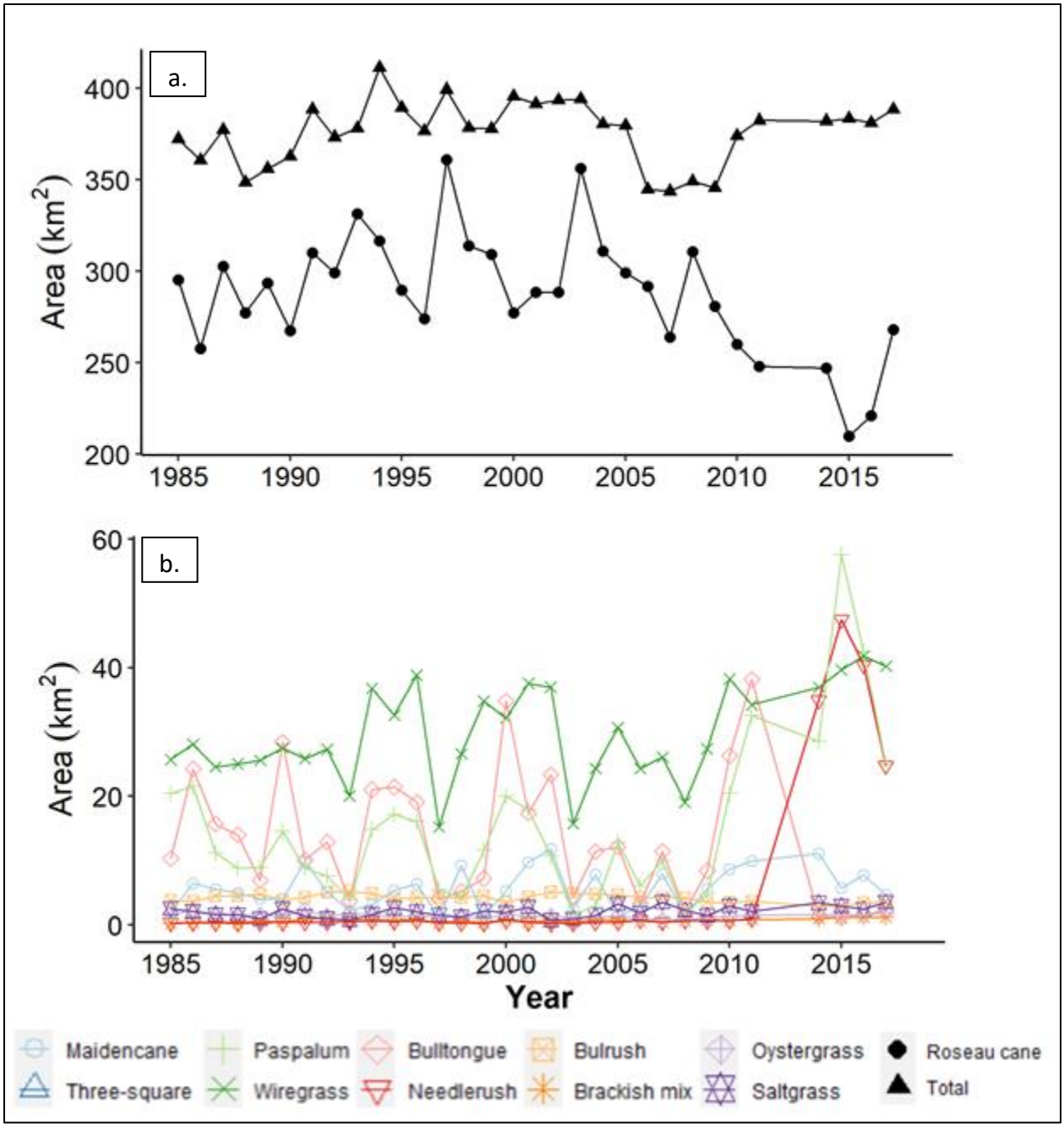

Figure 6. Area in square kilometers of (a). Roseau cane and total emergent herbaceous marsh vegetation community types and (b). Maidencane, Three-square, Paspalum, Wiregrass, Bulltongue, Needlerush, Bulrush, Brackish mix, Oystergrass, and Saltgrass community types in the Balize Delta, Louisiana, USA from 1985 to 2017

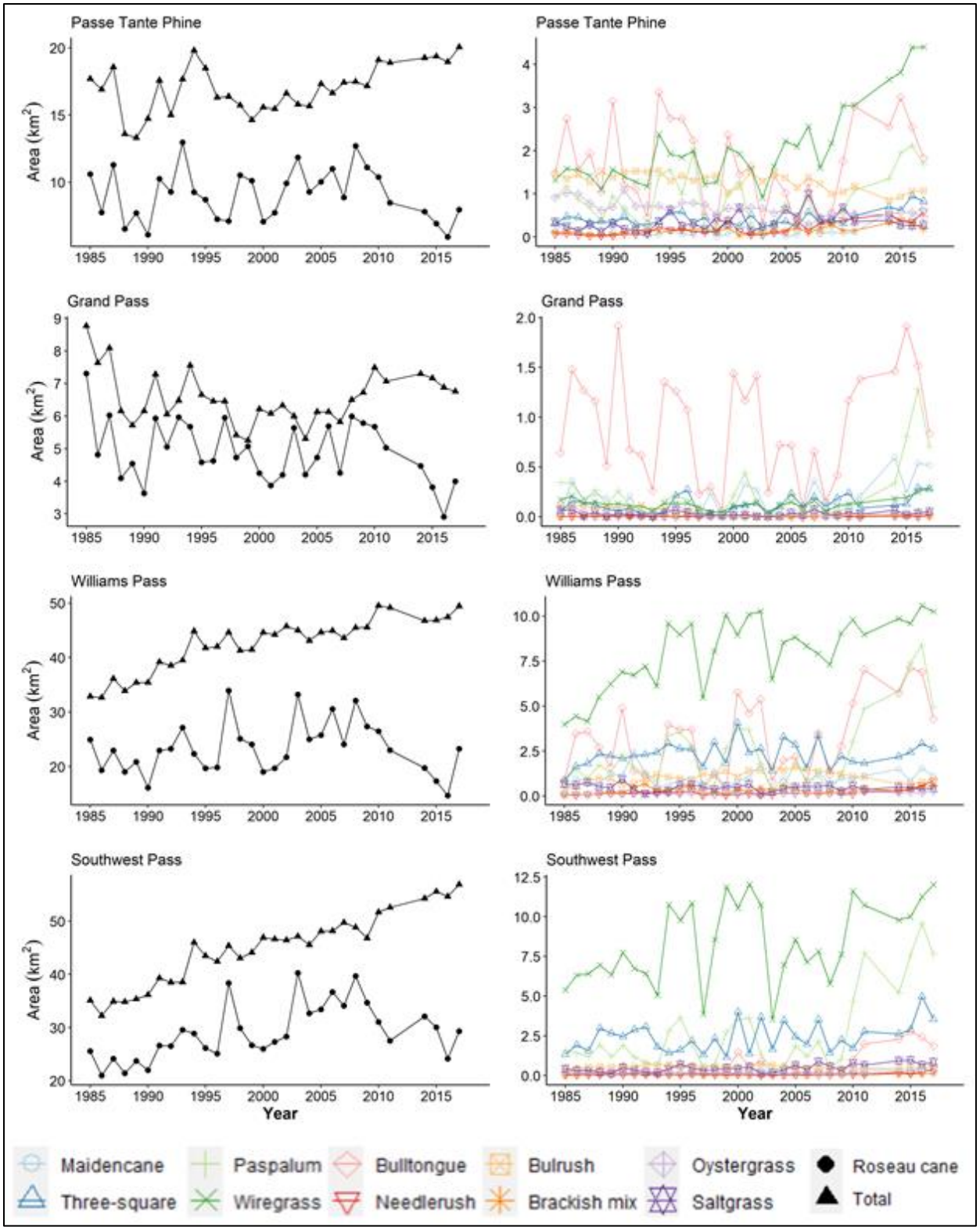

Figure 7. Area in square kilometers of Roseau cane, Maidencane, Three-square, Paspalum, Wiregrass, Bulltongue, Needlerush, Bulrush, Brackish mix, Oystergrass, Saltgrass and total community types in 10 subwatersheds of the Balize Delta, Louisiana, USA from 1985 to 2017. (fig. cont'd.)

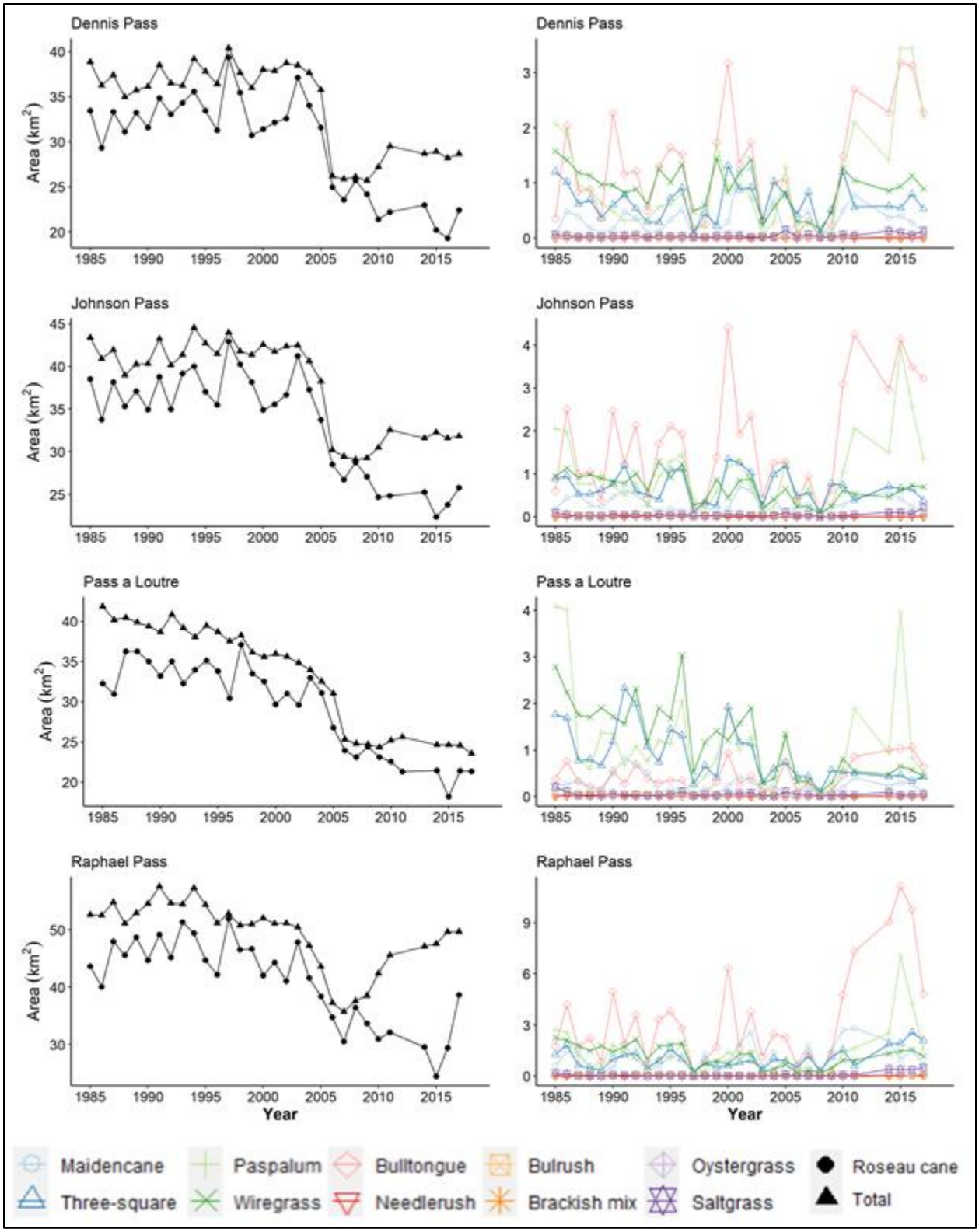

Figure 7 cont'd.

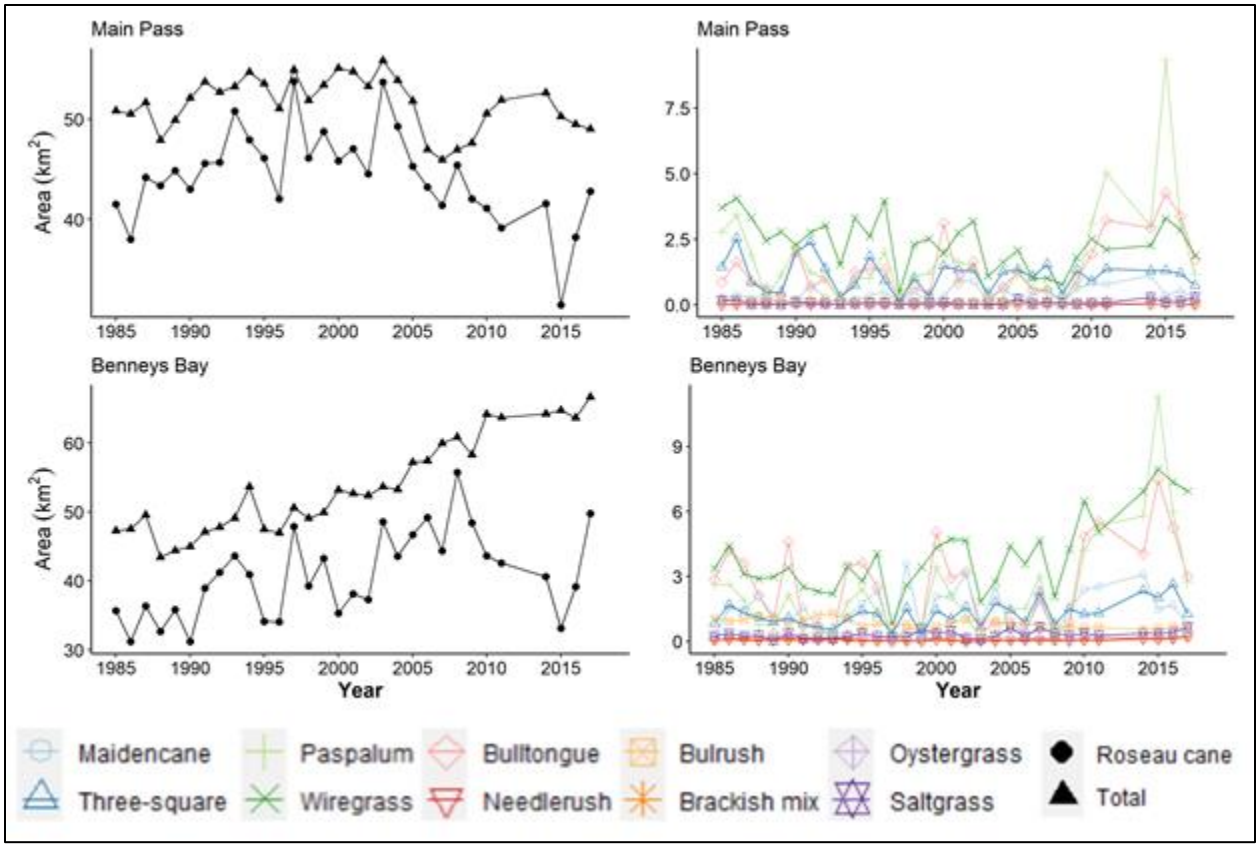

Figure 7 cont'd.

4.2. Fitted NDVI through time

Few obvious trends are seen in plotting the NDVI remainders through time. In most of the HUC12s, there are very low NDVI remainder values in 2005 and 2006. In six of the HUC12s, Pass Tante Phine, Grand Pass, Williams Pass, Southwest Pass, Dennis Pass, and Johnson Pass, a clustering of low values is seen around 2015.

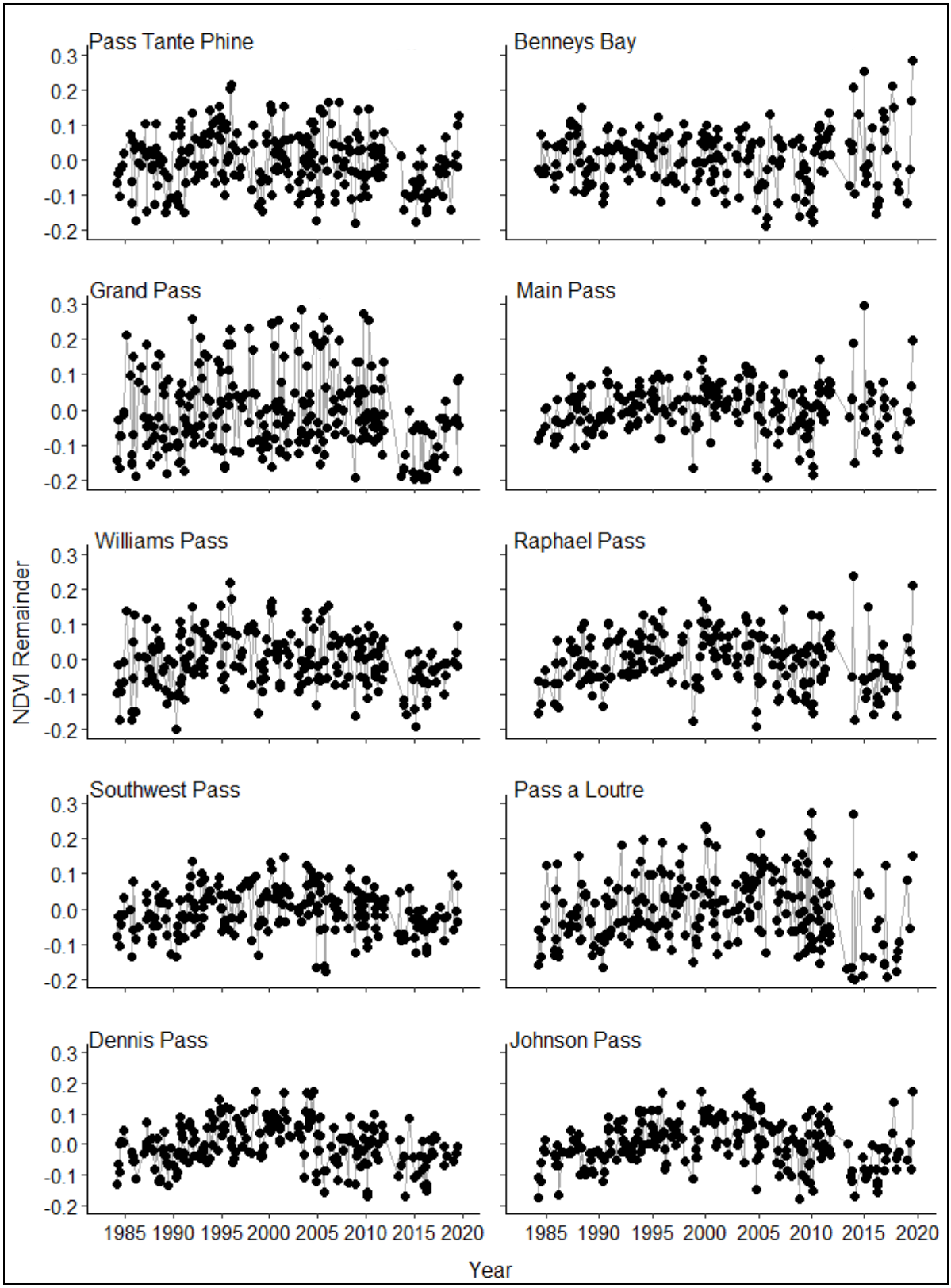

Figure 8. Remainders between harmonically fitted NDVI values and NDVI values for *Phragmites australis* from 1985 to 2019 for ten HUC12 (subwatersheds) within the Balize Delta

A penalized regression spline overlayed on NDVI remainders for each HUC12 shows the trends NDVI trends through time (Figure 9.). Fitted trends, as indicated by the r-squared values, for each HUC12 are very low, accounting for only a small amount of variation in the data. Each HUC12 has its own trend. In all HUC12s, except for Benneys Bay and Southwest Pass, a small drop in NDVI can be seen around 2013 to 2014. When the individual regression lines are averaged with weights assigned by *P. australis* area within the HUC12, we see NDVI trends for the basin as a whole (Figure 10.). The regression line reached three notable low values, -0.016 in 2006, -0.018 in 2009 and -0.047 in 2016. Declines began in late 2012 or early 2013, but were first noticed by managers in 2016, began in late 2012 or early 2013.

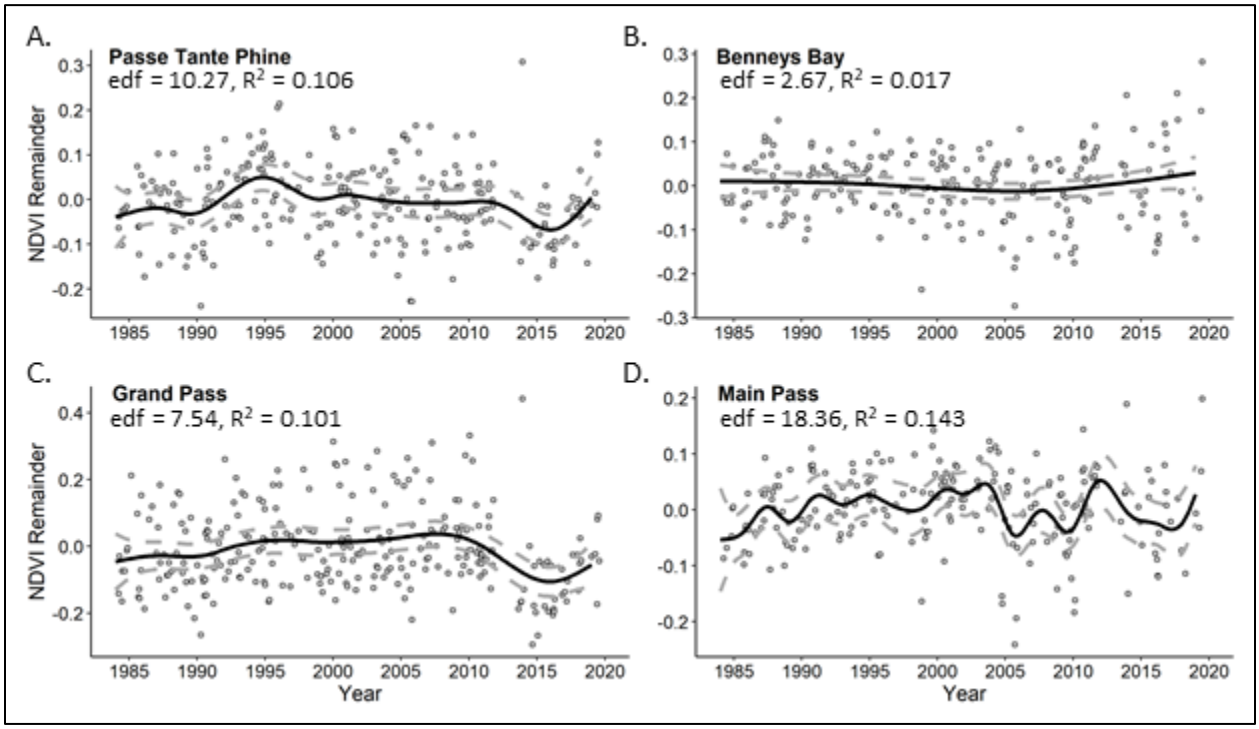

Figure 9. Remainders between harmonically fitted NDVI values and NDVI values from 1985 to 2019 with penalized regression smoothed spline, 95% confidence interval, effective degrees of freedom and r-squared values for ten HUC12 (subwatersheds) within the Balize Delta (fig. cont'd.)

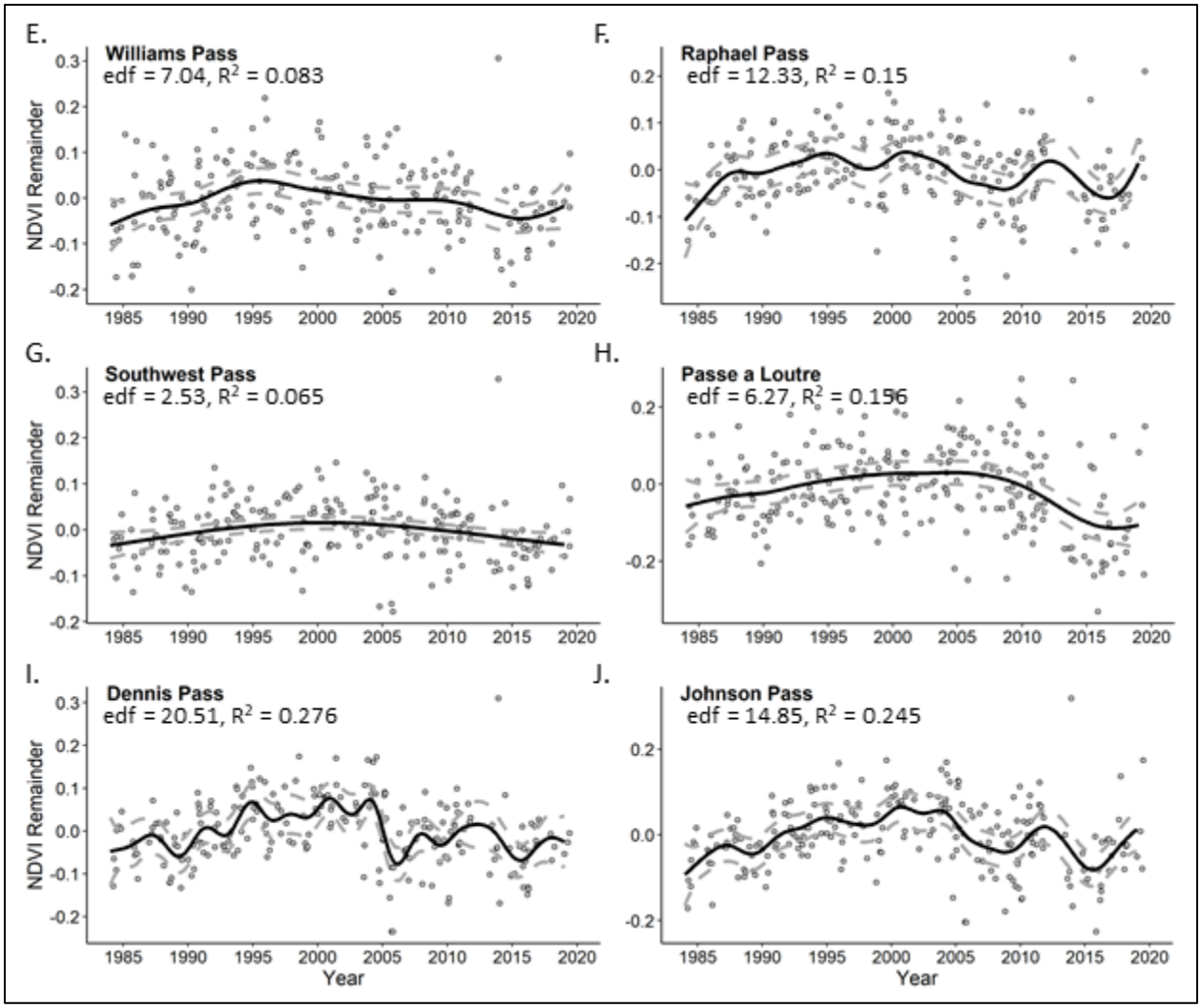

Figure 9 cont'd.

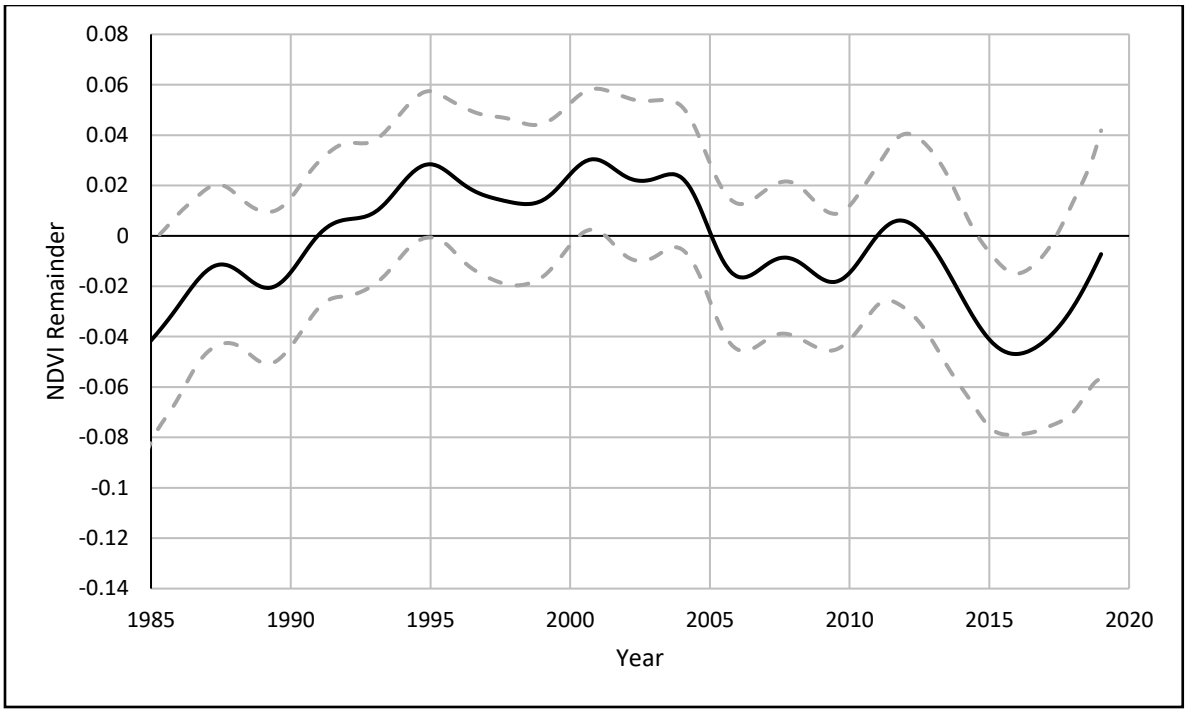

Figure 10. Area weighted mean of basin scale penalized regression smoothed spline for remainders of harmonically adjusted NDVI between 1985 and 2019

4.3. Seasonal difference from average

The collection of images created to calculate seasonal differences in the average of NDVI values did not show a definitive pattern of dieback (Figure 11.). The summer of 2013 composite had large areas of below average NDVI compared to a seasonal average throughout the Balize Delta. These areas remained near average throughout 2014 with some spots above and some below. By the winter of 2015 most of the area had above average NDVI values with a sparse distribution of below average values in the spring but with a more widespread distribution during fall 2015. Though the lower than average values were widespread, the magnitude of the values were only slightly below seasonal NDVI averages. Again, through the winter, NDVI values return to average. Then throughout 2016 and 2017, the majority of the area demonstrated above average NDVI, until dropping

below average in the winter and spring of 2018. The distribution of above and below average NDVI values were intermixed in the summer and fall of 2018 and winter of 2019, with a few areas of clouds that were not detected by the cloud masking method.

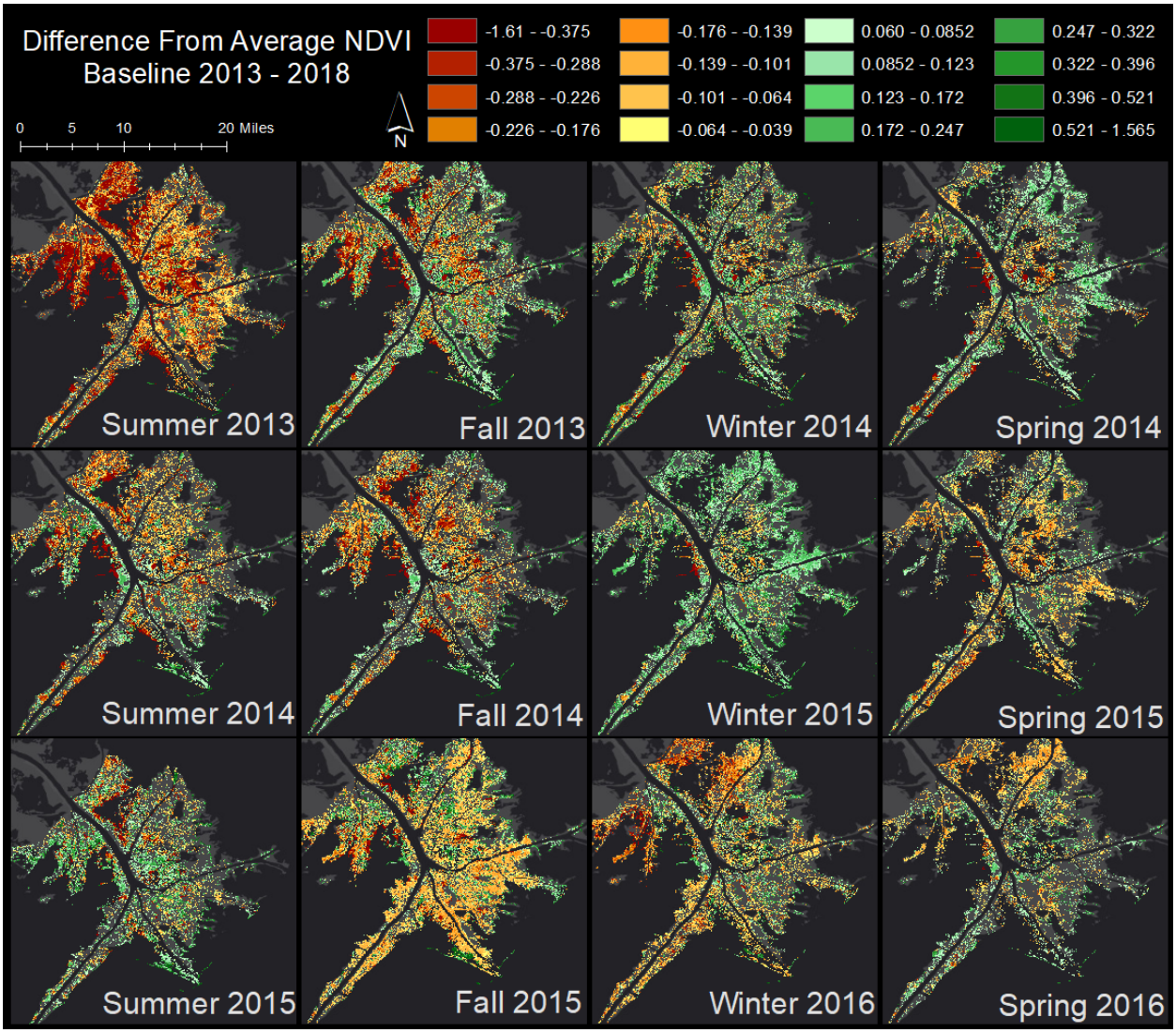

Figure 11. NDVI difference from average for each season between 2013 and 2019 with baseline as seasonal averages between 2013 and 2018 in the Balize Delta, Louisiana, USA
(fig. cont'd.)

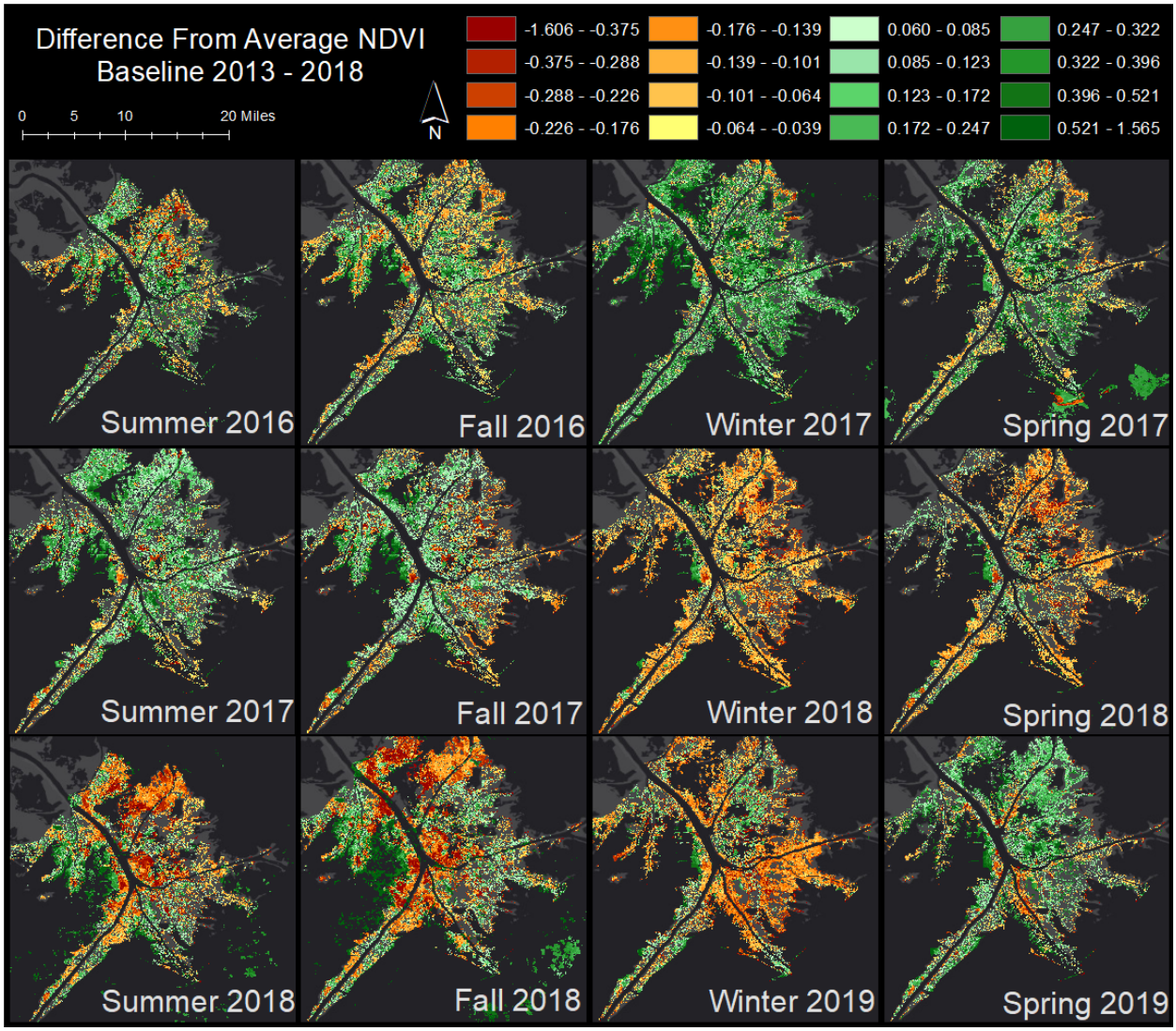

Figure 11 cont'd.

CHAPTER 5. DISCUSSION

Comparing helicopter-based observations of vegetation types to the remotely sensed-based classification of vegetation types that we generated suggests that classification based on satellite images was acceptably accurate. The two-step classification method used for identifying vegetation community types was successful with the first step of NLCD classification being 80% accurate (Table 7.) and the vegetation community type classification being 70% accurate (Table 8.). For each of these classifications, the accuracies for the classes of interest, emergent herbaceous marsh and *P. australis*, were higher than the average user accuracy at 89% and 75% respectively. A high user accuracy with a lower producer accuracy (82% for herbaceous marsh and 45% for *P. australis*), means that the classes were well detected by our classifiers, but the model may also include points of other classes in it. Because this was an imbalanced dataset, most of the points belong to one class and average accuracy may not be the best metric for measuring the effectiveness. The kappa statistic gives another metric to assess the reliability of the classification method, with a kappa of .575 for the NLCD classification, the model is in moderate agreement to the actual classes. For vegetation community type classification, a kappa of .634 shows that the model is in substantial agreement with the actual class data.

Accurately classifying vegetation types with remotely sensed data is challenging in wetlands because of overlaps in spectral signatures between wetlands and other land cover types and between different types of wetlands (Gluck et al., 1996). The individual methods used in this study are not novel and have been used in previous remote sensing studies, but the combination and application are innovative. Using harmonic analysis of trends in NDVI and

mNDWI provides a way to include seasonal trends at each location into the classification scheme. Each vegetation community type reacts differently throughout the growing season, the addition of these seasonal bands provides more information that is used to separate vegetation community types. Using PCA on raw sensor data results in images with uncorrelated variables that may be more interpretable than the original data (Singh and Harrison, 1985). PCA has been employed in remote sensing for change detection and used to extract wetland area from MODIS data with accuracies from 85 to 87% (Bansal et al., 2017). Again, including the bands resulting from PCA provides further information to accurately resolve vegetation types. The most common computer-based classification method used for the classification of wetlands in satellite images is unsupervised classification (Ozesmi and Bauer, 2002). Combining the results from harmonic analysis and PCA with both CART and random forest classifiers reduces the amount of overlap of spectral signatures allowing for further separation of wetland types. The ability to separate the major vegetation types increases our ability to look at smaller changes in a specific vegetation type. This multistep approach to classification may be helpful in other coastal environments to extract information on vegetation areas and extents, where sufficient imagery is available.

Remote sensing classification of wetland vegetation is a useful process for comparing fish and wildlife habitat between areas and/or over time, tracking changes in dominant species, and monitoring distributions of invasive species. *P. australis* has been separated from other wetland vegetation by methods using different combinations of elevation models, unmanned aerial vehicles, and high resolution data (Gilmore et al., 2008; Lin et al., 2015; Zhang et al., 2018). The classification methods used in this study allowed us to classify vegetation in imagery

dating to 1985, providing a historic view of *P. astralis* extent in the Balize Delta rather than one snapshot in time. The classification of *P. australis* allowed NDVI analysis to focus on the vegetation community of interest instead of all vegetation in the area.

From 1985 to 2005, the area of all vegetation types in the Balize Delta increased (Figure 6a.). While there was annual variability, as there is in most natural systems, the total area increased until 2005. This finding is consistent with land area change analysis that showed the Balize Delta having a net loss of land area overall from 1932 to 2016 but increasing in area between the early-1980s and the mid-2000s (Couvillion et al., 2017). One explanation for the increase in land area between 1985 and 2005 is the occurrence of crevasse-splays or cuts/breaks in the levee. Natural breaks can occur in levees after prolonged, high river discharge but have also been implemented as a restoration tool, a procedure that has occurred in the Balize Delta since at least the 1950s (Loga & Ensminger, 1958-1959). In 1978, a notable natural crevasse opened along Brant Bayou, a distributary in the Delta National Wildlife Refuge, and built over 12 km^2 of wetlands by 1990 (Boyer et al., 1997). Between 1983 and 1995, 24 crevasses were constructed within the Delta National Wildlife Refuge, with an average growth rate of 0.0476 km^2/year (Boyer et al., 1997). These constructed and natural breaks in the levee have increased wetland area as sediment laden water slows, dropping its load, which caused increasing sediment accretion followed by rapid vegetation colonization. These breaks build land in a similar manner but at a smaller spatial and temporal scale than the delta-lobe cycle.

Our finding that approximately 380 km^2 of herbaceous wetlands persisted in the Balize Delta from the 1985 to 2017, except for a temporary decline associated with Hurricane Katrina (Figure 4.), suggests that management and restoration there focused on promoting the river's

natural ability to create new wetlands might be a valuable addition to Louisiana's Master Plan for a Sustainable Coast. The 2012 and 2017 plans lack efforts to promote delta building in the Balize Delta even though such projects are among the most cost effective in coastal Louisiana (Boyer et al. 1997).

Until Hurricane Katrina, vegetation in the Balize Delta has been resilient to storms and hurricanes. In 1969, Hurricane Camille struck, having little effect on *P. australis* and significant recovery of other species within a year (Chabreck & Palmisano, 1973). However, the sharp decrease in overall vegetation in 2005 was most likely due to Hurricane Katrina, a Category 3 storm whose track intersected the Balize Delta. Hurricane Katrina's storm surge and flooding caused the destruction and weakening of coastal wetlands, including development of "shears", water bodies formed from the partial or complete removal of marsh vegetation; one 2.31 km^2 shear was identified along the east bank of South Pass in the Balize Delta (Barras, 2007). During this drop in total vegetation area, the area of *P. australis* increased, suggesting resilience of this community type to storms and perturbation. Between 2003 and 2013, forested wetlands, dominated by *Taxodium distichum* closer to the main channel and dominated by *Salix* ssp. farther from the main channel, have been replaced by *P. australis* (Figure 12.). The persistence of forested wetlands despite previous hurricanes (Chabreck & Palmisano, 1973) prior to the 2000s combined with the loss of forested wetlands following hurricanes since the early 2000s suggest that salinity stress and/or flooding stress has increased in the Balize Delta. Salinity and flooding would be expected to increase because of increases in subsidence and/or sea-level rise. Initially, salinity alone would be expected to increase because of delta backstepping but

eventually flooding would increase as sedimentation and vertical accretion declined (Bentley et al. 2016).

Increases in Paspalum and Needlrush types appear to have coincided with declines in *P. australis* (Figure 6.). This increase in Needlerush might not actually represent increases in *J. romerianus*, which is rare in the Balize Delta, but might instead represent changes in other species within the Needlerush vegetation community type or species with similar spectral signatures.

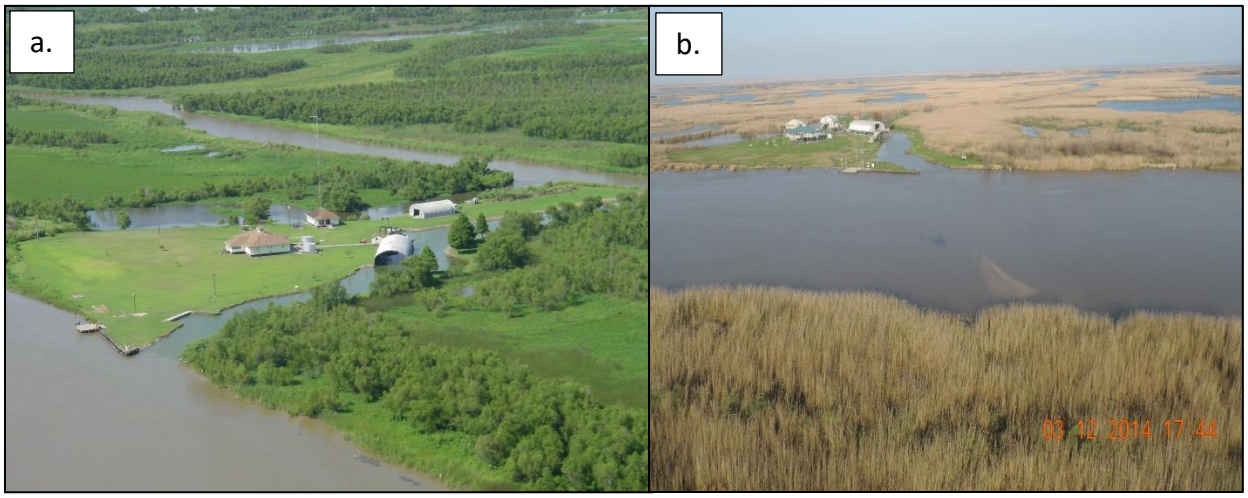

Figure 12. View of Louisiana Department of Wildlife and Fisheries camp located on Dennis Pass, Balize Delta, LA in (a.) 2003 with forested wetlands and (b.) 2014 with *P. australis* in place of woody vegetation *Source:* personal photos Curtis Richardson (a.) and Andy Nyman (b.)

Interesting spatial patterns emerged when vegetation type classifications were separated by HUC12s (Figure 7.). The HUC12s located further upstream (Passe Tante Pine, Grand Pass and Benney's Bay) appear to gain total vegetation area, which is consistent with the delta backstepping predicted by Bentley et al (2016). Downstream however, only Southwest Pass and Williams Pass have an increase in vegetation area. The Southwest Pass HUC12 actually is a receiving basin for numerous artificial uncontrolled sediment diversions from South Pass;

Williams Pass contains marsh creation projects from dredged sediments as well as receiving sediment from the West Bay Sediment Diversion. Total vegetation in Main Pass and Raphael Pass, located in the middle portion of the Balize Delta, is remaining constant while the most downstream HUC12s are losing vegetation (Pass a Loutre, Johnson Pass, and Dennis Pass). These spatial differences could be associated with the natural subdelta cycle driven by subsidence (Wells and Coleman, 1987) and/or an acceleration of the transgressional delta process caused by an accelerated sea-level rise combined with subsidence (Bentley et al. 2016).

The area of vegetation community type by HUC12 gives a slightly better view of what is happening to areas of other vegetation while *P. australis* has decreased. Predicting vegetation response after the removal or dieback of *P. australis* was outside the scope of this study. However, the vegetation changes in those areas are of great concert to managers and researchers. The three most likely outcomes after the dieback of *P. australis* in an area are: *P. australis* recovers, the area converts to open water, or the area is colonized by other vegetation. The Louisiana Coastal Master Plan uses vegetation model to predict changes in vegetation under different restoration conditions (Visser et al., 2013). This model is focused on the salinity and water levels that effect the establishment and mortality of different species and which species are present on the landscape to establish open areas (Visser et al., 2013). Dieback areas of *P. australis* will respond differently depending on their elevation and average salinities.

NDVI of vegetation canopies has become one of the most valuable remote sensing techniques for regional and ecosystem-scale environmental research and management. NDVI correlates well with vegetation productivity, making it useful for a variety of application of

ecological importance (Reed et al., 1994). Water inundation plays an important role in ecosystem dynamics of wetland environments and can lower observed NDVI values. In areas where the marsh canopy covers most ground, the effect of subcanopy flooding on NDVI is minimal. Value compositing, step-wise logistic regression, curve-fitting, and weighted least-squares linear regression are among the most common practices for smoothing NDVI time-series data (Holben, 1986; Olsson and Eklundh, 1994; Van Dijk et al., 1987; Zhang et al., 2003). Seasonal images were composited based on an average NDIV value to reduce the effect of water on NDVI values. Through harmonic analysis and the addition of a penalized regression spline, general trends in NDVI were examined rather than raw NDVI. These steps allowed me to reduce the effect one flooded image may have on the analysis.

After harmonic analysis of NDVI, the difference between the fitted values and the obseved values appeared to have no trend (Figure 8.). Individual low values in 2005 and 2009 were most likely a result of Hurricanes Katrina and Gustav respectively. Benneys Bay, Main Pass, Raphael Pass, and Pass a Loutre varied widely between 2015 and 2020. This varriation persisted in the northeast area of the Balize Delta but not the rest.

The addition of the penalized regression spline provides a better understanding of *P. australis* NDVI trends through time (Figure 9.). Each HUC12 has it's own patterns, influenced by the vegetation amount, vegetation vigor, and water levels within that HUC12. Within all HUC12s, except Southwest Pass and Benneys Bay, NDVI began declining before 2015 and reaching a minimum around 2016 (Figure 9.). The onset of those declines was not simulatneous however. Those declines appear to have begun sooner, around 2010, in HUC12's where the remainder was near 0 before the decline began: Passe Tante Phine, Grand Pass, Williams Pass,

and Dennis Pass. Those declines appear to have begun later, around 2013 in HUC12's where the remainder was positive before the declines began: Main Pass, Raphael Pass, and Johnson Pass. This pattern is consistent with dieback being caused by multiple stresses that vary across the Balize Delta.

Averaging all of the HUC12's together obscures differences in health before dieback began and differences in the timing of dieback. However, the area weighted mean of the penalized regression well illuminates changes that affected the Balize Delta simultaneously,such as the Hurricanes Katrian and Gustav in 2005 and 2008 respectively (Figure 10.). From 1985 to the early 2000s there was a general upward trend in NDVI. One interpretation of this trend is a general emergent wetland growth described previously. A marked decrease in *P. australis* NDVI over the basin (Figure 10.) was attributed to Hurricane Katrina whose storm surge and high winds caused severe damage to the marsh (Barras, 2007). The regression line begins to curve earlier than 2005 because statitistical solutions cause the splines to curve in anticipation of fitting the low values to come. The vegetation began to recover from Hurricane Katrina a little before another small decreas that was attributed to Hurrican Gustav. From 2009 to 2013 there was once again recovery, with a maximum of 0.006 in 2012. The largest decrease within the period began just before 2012, reaching its minimum of -0.046 in 2016 before moving towards recovery though 2019. Once again, the regression line begins changing in anticipation of fitting the future points, but the overall trends indicated that the dieoff event could have began as early as 2014 with recovery occuring onward from 2016. Photos from March of 2014 (Figure 12b.) show what was then believed to be typical winter scenescense but probably could be attributed to dieback.

The seasonal NDVI difference from average images of all community types from 2013-2019 did not have a coherent or interpretable pattern (Figure 11.). It is possible that too many of these images are contaminated by clouds, especially in a humid, subtropical location like Louisiana. Cloud recognition methods are not perfect; cloudy pixels may miss being flagged in the pixel_qa band. While the use of a median composite helps to mitigate these issues, we see in Figure 11 (Spring 2017, Summer 2018, and Fall 2018) that clouds can still contaminate the analysis.

For these images (Figure 11.), the area was masked to land but not to *P. australis*, therefore they may include signals from other vegetation. If a *P. australis* mask was used however, we may miss areas that were converted to other vegetation or open water. Neither method is wrong, each provides different information. While masking to just *P. australis* for a particular year, we get an indication of NDVI of *P. australis* in particular. This method is useful for analyzing relative health of existing *P. australis* without focusing on converted areas. In a dieback scenario, the area lost may be an important piece to consider.

Tracking NDVI through time is useful for identifying large decreases in plant health and vigor, *in situ* measurements help to corroborate or fill in details. After identification of *N. biwakoensis* in the Balize Delta, efforts began to understand the role of the scake in the dieback of *P. australis* (Knight et al., 2018). A series of transects have been revisited in the Balize Delta, though the spatial scale and variables measured do not relate well to the remotely sensed data. The NDVI calculated from satelite images is from a top down view, which correlate little with metrics such as the verticle percent green on a stem have little correlation. On sampling trips to the Balize Delta in 2018 and 2019, I observed leafy and healthy looking *P. australis* stems

containing high densities of *N. biwakoensis*. During that time, NDVI values and the area of total vegetation and *P. australis* was increasing (Figure 6., Figure 10.). This period of recovery coincide with ongoing *N. biwakoensis* infestation, indicating that perhaps there are multiple stressors interacting to produce dieback symptoms.

Dieback of *P. australis* in Europe has been has been attributed to multiple stressors including phytotoxins in the sediment and eutrophication (Armstron et al., 1996; van der Putten et al., 1997). Other factors such as insects, fungal infection, and mechanical damage may play a role (Armstrong et al. 1996). In China, removal of stems, flooding in winter and spring, and removal of dead leaves are uses a methods to control the populations of *N. biwakoensis* in *P. australis* beds (Shen et al., 1995). Greenhouse studies are underway looking at the role of *N. biwakoensis* and salinity on *P. australis* health, these will provide important insight for managers.

REFERENCES

Able, K. W., Hagan, S. M., & Brown, S. A. (2003). Mechanisms of marsh habitat alteration due to *Phragmites*: Response of young-of-the-year mummichog (*Fundulus heteroclitus*) to treatment for *Phragmites* removal. *Esuaries*, *26*(2B), 484–494. https://doi.org/10.1007/BF02823725

Armstrong, J, Afreen-Zobayed, F., & Armstrong, W. (1996). *Phragmites* die-back: Sulphide-and acetic acid-induced bud and root death, lignifications, and blockages within aeration and vascular systems. New *Phytologist*, 134(4), 601-614. https://doi.org/10.1111/j.1469-8137.1996.tb04925.x

Armstrong, J, Armstrong, W., Armstrong, I. B., & Pittaway, G. R. (1996). Senescence, and phytotoxin, insect, fungal and mechanical damage: factors reducing convective gas-flows in *Phragmites australis*. *Aquatic Botany* 54(2-3), 211-226. https://doi.org/10.1016/0304-3770(96)82384-9

Armstrong, Jean, & Armstrong, W. (2001). An overview of the effects of phytotoxins on Pragmites australis in relation to die-back. *Aquatic Botany*, *69*(2–4), 251–268. https://doi.org/10.1016/S0304-3770(01)00142-5

Bansal, S., Katyal, D., Garg, J. K. (2017). A novel strategy for wetland area extraction using multispectral MODIS data. *Remote Sensing of Environment, 200:* 183-205. https://doi.org/10.1016/j.rse.2017.07.034

Baranov, Y. I., & Lafferty, W. J. (2012). The water vapour self-and water-nitrogen continuum absorption in the 1000 and 2500 cm-1 atmospheric windows. *Philosophical Transactions: Mathematical, Physical and Engineering Sciences*, *370*(1968), 2578–2589. https://doi.org/10.1098/rsta.2011.0234

Barras, J. A. (2007). Land area changes in coastal Louisiana after Hurricanes Katrina and Rita. *US Geological Survey Circular*, *1306*, 97–112. https://doi.org/10.3133/cir13065b

Bart, D., Burdick, D., Chambers, R., Hartman, J. M. (2006). Human facilitation of *Phragmites australis* invasions in tidal marshes: A review and synthesis. *Wetlands Ecology and Management, 14*: 53-65. https://doi.org/10.1007/s11273-005-2566-z

Belgiu, M., & Drăgu, L. (2016). Random forest in remote sensing: A review of applications and future directions. *ISPRS Journal of Photogrammetry and Remote Sensing*, *114*, 24–31. https://doi.org/10.1016/j.isprsjprs.2016.01.011

Bentley, S. J., Blum, M. D., Maloney, J., Pond, L., Paulsell, R. (2016). The Mississippi River source-to-sink system: Perspectives on tectonic, climatic, and anthropogenic influences, Miocene to Anthropocene. *Earth-Science Reviews, 153:* 139-174. https://doi.org/10.1016/j.earscirev.2015.11.001

Bera, P. P., Francisco, J. S., & Lee, T. J. (2010). Design strategies to minimize the radiative efficiency of global warming molecules. *Proceedings of the National Academy of Sciences of the United States of America*, *107*(20), 9049–9054. https://doi.org/10.1073/pnas.0913590107

Blum, M. D., & Roberts, H. H. (2012). The Mississippi Delta region: Past, present, and future. *Annual Review of Earth and Planetary Sciences*, *40*, 655–683. https://doi.org/10.1146/annurev-earth-042711-105248

Boesch, D. F., Josselyn, M. N., Mehta, A. J., Morris, J. T., Nuttle, W. K., Simenstad, C. A., & Swift, D. J. P. (1994). Scientific assessment of coastal wetland loss, restoration and management in Louisiana. *Journal of Coastal Research*, *Special Issue 20*, 15–36. Retrieved March 11, 2020, from www.jstor.org/stable/25735693

Boyer, M. E., Harris, J. O., & Turner, R. E. (1997). Constructed crevasses and land gain in the Mississippi River delta. *Restoration Ecology*, *5(1)*, 85-92. https://doi.org/10.1046/j.1526-100X.1997.09709.x

Breiman, L. (2001). Random forests. *Machine Learning*, *45*(1), 5–32. https://doi.org/10.1023/A:1010933404324

Breiman, L., Friedman, J. H., Olshen, R. A., & Stone, C. J. (1984). *Classification and Regression Trees*. Taylor & Francis Group.

Butt, N., Seabrook, L., Maron, M., Law, B. S., Dawson, T. P., Syktus, J., & Mcalpine, C. A. (2015). Cascading effects of climate extremes on vertebrate fauna through changes to low-latitude tree flowering and fruiting phenology. *Global Change Biology*, *21*, 3267–3277. https://doi.org/10.1111/gcb.12869

Cahoon, D. R., Reed, D. J., & Day, J. W. (1995). Estimating shallow subsidence in microtidal salt marshes of the southeastern United States: Kaye and Barghoorn revisited. *Marine Geology*, *128*, 1–9. https://doi.org/10.1016/0025-3227(95)00087-F

Cardoch, L., Day, J. W., & Ibàñez, C. (2002). Net primary productivity as an indicator of sustainability in the Ebro and Mississippi deltas. *Ecological Applications*, *12*(4), 1044–1055. https://doi.org/10.1890/1051-0761(2002)012[1044:NPPAAI]2.0.CO;2

Chabreck, R H. (1970). *Marsh zones and vegetative types in the Louisiana coastal marshes*. [Doctoral dissertation, Louisiana State University and Agricultural and Mechanical College]. LSU Digital Commons.

Chabreck, R.H., and Linscombe, G., 1978, Vegetative type map of the Louisiana coastal marshes: Baton Rouge, Louisiana Department of Wildlife and Fisheries.

Chabreck, R.H., and Linscombe, G., 1988, Vegetative type map of the Louisiana coastal marshes: Baton Rouge, Louisiana Department of Wildlife and Fisheries, set of 10 maps.

Chabreck, R.H., and Linscombe, G., 1997, Vegetative type map of the Louisiana coastal marshes: Baton Rouge, Louisiana Department of Wildlife and Fisheries.

Chabreck, Robert H., & Palmisano, A. W. (1973). The effects of Hurricane Camille on the marshes of the Mississippi River delta. *Ecology*, *54*(5), 1118–1123. https://doi.org/10.2307/1935578

Chander, G., Markham, B. L., & Helder, D. L. (2009). Summary of current radiometric Calibration coefficients for Landsat MSS, TM, ETM+, and EO-1 ALI sensors. *Remote Sensing of Environment*, *113*(5), 893–903. https://doi.org/10.1016/j.rse.2009.01.007

Chavez, P. S., Sides, S. C., & Anderson, J. A. (1991). Comparison of three different methods to merge multiresolution and multispectral data: Landsat TM and SPOT panchromatic. *Photogrammetric Engineering and Remote Sensing*, *57*(3), 295–303. https://doi.org/10.1306/44b4c288-170a-11d7-8645000102c1865d

Chuvieco, E., & Huete, A. (2010). *Fundamentals of Satellite Remote Sensing*. Taylor and Francis Group.

Ciddor, P. E. (1996). Refractive index of air: New equations for the visible and near infrared. *Applied Optics*, *35*(9), 1566. https://doi.org/10.1364/ao.35.001566

Coleman, J.M. 1981. Deltas processes of deposition and models for exploration. Burgess Publishing Co., Minneapolis, MN.

Coleman, J. M. (1988). Dynamic changes and depositional processes in the Mississippi River delta. *Geological Society of America Bulletin*, *100*, 999–1015.

Coleman, J. M., Huh, O. K., & Braud Jr., D. (2008). Wetland loss in world deltas. *Journal of Coastal Research*, *24*(1A), 1–14. https://doi.org/10.2112/05-0607.1

Coleman, J. M., Roberts, H. H., & Stone, G. W. (1998). Mississippi River Delta: An overview. *Journal of Coastal Research*, *14*(3), 698–716. https://www.jstor.org/stable/4298830

Cook, C. E., McCluskey, A. M., & Chambers, R. M. (2018). Impacts of invasive *Phragmites australis* on diamondback terrapin nesting in Chesapeake Bay. *Estuaries and Coasts*, *41*, 966–973. https://doi.org/10.1007/s12237-017-0325-z

Costanza, R., de Groot, R., Sutton, P., van der Ploeg, S., Anderson, S. J., Kubiszewski, I., Farber, S., Turner, R. K. (2014). Changes in the global value of ecosystem services. *Global Environmental Change, 26*, 152-158. https://doi.org/10.1016/j.gloenvcha.2014.04.002

Couvillion, B., Barras, J., Steyer, G., Sleavin, W., Fischer, M., Beck, H., Trahan, N., Griffin, B., & Heckman, D. (2011). *Land Area Change in Coastal Louisiana from 1932 to 2010: U.S. Geological Survey Scientific Investigations Map 3164*.

Couvillion, B. R., Beck, H., Schoolmaster, D. R., & Fischer, M. (2017). *Land area change in coastal Louisiana 1932 to 2016: U.S. Geological Survey Scientific Investigations Map 3381*. U.S. Geological Survey. https://doi.org/10.3133/sim3381

CPRA (Coastal Protection and Restoration Authority). (2012). *Louisiana's Comprehensive Master Plan for a Sustainable Coast*.

Day, J. W., Boesch, D. F., Clairain, E. J., Kemp, G. P., Laska, S. B., Mitsch, W. J., Orth, K., Mashriqui, H., Reed, D. J., Shabman, L., Simenstad, C. A., Streever, B. J., Twilley, R. R., Watson, C. C., Wells, J. T., & Whigham, D. F. (2007). Restoration of the Mississippi Delta: Lessons from Hurricanes Katrina and Rita. *Sience*, *315*(5819), 1679–1684. https://doi.org/10.1126/science.1137030

Earth Resources Observation and Science (EROS) Data Center. (2019a). *Landsat 4-7 Surface Reflectance (Ledaps) Product Guide* (Issue LSDS-1370). U.S. Geological Survey.

Earth Resources Observation and Science (EROS) Data Center. (2019b). *Landsat 8 Surface Reflectance Code (LASRC) Poduct Guide* (Issue LSDS-1368, p. 2.0). U.S. Geological Survey.

Eastman, J. R., & Fulk, M. (1993). Long sequence time series evaluation using standardized pricipal components. *Photogrammetric Engineering & Remote Sensing*, *59*(8), 1307–1312.

Eilers, P. H. C., & Marx, B. D. (1996). Flexible smoothing with B-splines and penalties. *Statistical Science*, *11*(2), 89–121. https://doi.org/10.1214/ss/1038425655

Eller, F., Skálová, H., Caplan, J. S., Bhattarai, G. P., Burger, M. K., Cronin, J. T., Guo, W. Y., Guo, X., Hazelton, E. L. G., Kettenring, K. M., Lambertini, C., McCormick, M. K., Meyerson, L. A., Mozdzer, T. J., Pyšek, P., Sorrell, B. K., Whigham, D. F., & Brix, H. (2017). Cosmopolitan species as models for ecophysiological responses to global change: The common reed *Phragmites australis*. *Frontiers in Plant Science*, *8,* 1833. https://doi.org/10.3389/fpls.2017.01833

Elmer, W. H., Useman, S., Schneider, R. W., Marra, R. E., LaMondia, J. A., Mendelssohn, I. A., Jiménez-Gasco, M. M., & Caruso, F. L. (2013). Sudden vegetation dieback in Atlantic and Gulf coast salt marshes. *Plant Disease*, *97*(4), 436–445. https://doi.org/10.1094/PDIS-09-12-0871-FE

Gilmore, M. S., Wilson, E. H., Barrett, N., Civco, D. L., Prisloe, S., Hurd, J. D., Chadwick, C. (2008). Integrating multi-temporal spectral and structural information to map wetland vegetation in a lower Connecticut River tidal marsh. *Remote Sensing of the Environment*, 112, 4048-4060. https://doi.org/10.1016/j.rse.2008.05.020

Gluck, M., Rempel, R., and Uhlig, P. (1996). An evaluation of remote sensing for regional wetland mapping applications. *Ontario Forest Research Institute, Canadian Forest Research Institute*. Sault Ste. Marie: Ontario Forest Research Institute.

Goodman, P. J., & Williams, W. T. (1961). Investigations into 'die-back' in *Spartina townsendii*. *Journal of Ecology*, *49(2)*, 391–398. https://doi.org/10.2307/2257271

Goward, S. N., Tucker, C. J., & Dye, D. G. (1985). North American vegetation patterns observed with the NOAA-7 advanced very high resolution radiometer. *Vegetatio*, *64*, 3–14. https://doi.org/10.1007/BF00033449

Hall-Beyer, M. (2003). Comparison of single-year and multiyear NDVI time series principal components in cold temperate biomes. *IEEE Transactions on Geoscience and Remote Sensing*. *41*(11), 2568–2574. https://doi.org/10.1109/TGRS.2003.817274

Hansen, R. M. (1978). Shasta ground sloth food habits , Rampart Cave , Arizona. *Paleobiology. 4(3)*, 302-319. https://www.jstor.org/stable/2400207

Hauber, D. P., Saltonstall, K., White, D. A., & Hood, C. S. (2011). Genetic variation in the common reed, *Phragmites australis*, in the Mississippi River delta marshes: Evidence for multiple introductions. *Estuaries and Coasts*, *34*, 851–862. https://doi.org/10.1007/s12237-011-9391-9

Havens, K. J., Berquist, H., & Priest, W. I. (2003). Common reed grass, *Phragmites australis*, expansion into constructed wetlands: Are we mortgaging our wetland future? *Estuaries*, *26*(2B), 417–422. https://doi.org/10.1007/BF02823718

Holben, B. N. (1986). Characteristics of maximum-value composite images from temporal AVHRR data. *International Journal of Remote Sensing, 7(11):* 1417-1434. https://doi.org/10.1080/01431168608948945

Houghton, J. T. (1979). Greenhouse effects of some atmospheric constituents. *Philosophical Transactions of the Royal Society of London. Series A, Mathematical and Physical Sciences*, *290*(1376), 515–521. https://www.jstor.org/stable/75087

Hughes, A. L. H., Wilson, A. M., & Morris, J. T. (2012). Hydrologic variability in a salt marsh: Assessing the links between drought and acute marsh dieback. *Estuarine, Coastal and Shelf Science*, *111*, 95–106. https://doi.org/10.1016/j.ecss.2012.06.016

Jackson, R. D., Slater, P. N., & Pinter, P. J. (1983). Discrimination of growth and water stress in wheat by various vegetation indices through clear and turbid atmospheres. *Remote Sensing of Environment*, *13*, 187–208. https://doi.org/10.1016/0034-4257(83)90039-1

Jakubauskas, M. E., Legates, D. R., & Kastens, J. H. (2001). Harmonic analysis of time-series AVHRR NDVI data. *Photogrammetric Engineering and Remote Sensing*, *67*(4), 461–470.

Jensen, J. R. (2005). *Introductory digital image processing: A remote sensing perspective, 3rd edition* (D. E. Kaveney (ed.); 3rd ed.). Prentice Hall Logicon Geodynamics, Inc.

Jin, S., Homer, C., Yang, L., Danielson, P., Dewitz, J., Li, C., Zhu, Z., Xian, G., & Howard, D. (2019). Overall methodology design for the United States National Land Cover Database 2016 products. *Remote Sensing*, *11*(24), 2971. https://doi.org/10.3390/rs11242971

Keddy, P. A., Fraser, L. H., Solomeshch, A. I., Junk, W. J., Campbell, D. R., Arroyo, M. T. K., & Alho, C. J. R. (2009). Wet and wonderful: The world's largest wetlands are conservation priorities. *BioScience*, *59*(1), 39–51. https://doi.org/10.1525/bio.2009.59.1.8

Keller, B. E. M. (2000). Plant diversity in *Lythrum*, *Phragmites*, and *Typha* marshes, Massachusetts, U.S.A. *Wetlands Ecology and Management*, *8*(6), 391–401. https://doi.org/10.1023/A:1026505817409

Kettenring, K. M., de Blois, S., & Hauber, D. P. (2012). Moving from a regional to a continental perspective of *Phragmites australis* invasion in North America. *AoB Plants*. https://doi.org/10.1093/aobpla/pls040

Kettenring, K. M., Mock, K. E., Zaman, B., & McKee, M. (2016). Life on the edge: reproductive mode and rate of invasive *Phragmites australis* patch expansion. *Biological Invasions*, *18*, 2475–2495. https://doi.org/10.1007/s10530-016-1125-2

Kiviat, E., & Hamilton, E. (2001). *Phragmites* use by native North Americans. *Aquatic Botany*, *69*(2–4), 341–357. https://doi.org/10.1016/S0304-3770(01)00147-4

Knight, I. A., Wilson, B. E., Gill, M., Aviles, L., Cronin, J. T., Nyman, J. A., Schneider, S. A., & Diaz, R. (2018). Invasion of *Nipponaclerda biwakoensis* (*Hemiptera: Aclerdidae*) and *Phragmites australis* die-back in southern Louisiana, USA. *Biological Invasions*, *20*, 2739–2744. https://doi.org/10.1007/s10530-018-1749-5

Kotchenova, S. Y., Vermote, E. F., Matarrese, R., & Klemm, F. J. (2006). Validation of a vector version of the 6S radiative transfer code for atmospheric correction of satellite data. Part I: Path radiance. *Applied Optics*, *45*(26), 6762–6774. https://doi.org/10.1364/AO.45.006762

Lambertini, C., Mendelssohn, I. A., Gustafsson, M. H. G., Olesen, B., Riis, T., Sorrell, B. K., & Brix, H. (2012). Tracing the origin of Gulf Coast *Phragmites* (*Poaceae*): A story of long-distance dispersal and hybridization. *American Journal of Botany, 99(3)*, 538-551. https://doi.org/10.3732/ajb.1100396

Leatherman, M.L. 1970. A vegetative study of the Sawdust Bend area, Plaquemines Parish, Louisiana. M.S. Thesis. Louisiana State University.

Lin, W., Chen, G., Guo, P., Zhu, W., Zhang, D. (2015). Remote-sensed monitoring of dominant plant species distribution and dynamics at Jiuduansha Wetland in Shanghai, China. *Remote Sensing, 7*, 10227-10241. https://doi.org/10.3390/rs70810227

Lissner, J., & Schierup, H.-H. (1997). Effects of salinity on the growth of *Phragmites australis*. *Aquatic Botany*, *55(4)*, 247–260. https://doi.org/10.1016/S0304-3770(96)01085-6

Lloyd, F. E., & Tracy, S. M. (1901). The insular flora of Mississippi and Louisiana. *Bulletin of the Torrey Botanical Club*, *28*(2), 61–101. https://doi.org/10.2307/2477884

Loga, E. W., & Ensminger, A. B. (1958-59). Pass-a-Loutre waterfowl management area. *Louisiana Wildlife and Fisheries Eigth Biennial Report*, 149-152.

Maiersperger, T. K., Scaramuzza, P. L., Leigh, L., Shrestha, S., Gallo, K. P., Jenkerson, C. B., & Dwyer, J. L. (2013). Characterizing LEDAPS surface reflectance products by comparisons with AERONET, field spectrometer, and MODIS data. *Remote Sensing of Environment*, *136*, 1–13. https://doi.org/10.1016/j.rse.2013.04.007

Major, D. J., Baret, F., & Guyot, G. (1990). A ratio vegetation index adjusted for soil brightness. *International Journal of Remote Sensing*, *11*(5), 727–740. https://doi.org/10.1080/01431169008955053

Marks, M., Lapin, B., & Randall, J. (1994). *Phragmites australis* (*P. communis*): Threats, management, and monitoring. *Natural Areas Journal*, *14*(4), 285-294.

Marsh, A., Blum, L. K., Christian, R. R., Ramsey, E., & Rangoonwala, A. (2016). Response and resilience of *Spartina alterniflora* to sudden dieback. *Journal of Coastal Conservation*, *20*(4), 335–350. https://doi.org/10.1007/s11852-016-0445-9

Mather, P. M. (1987). *Computer Processing of Remotely-Sensed Images*. John Wiley & Sons.

Matthews, E., Fung, I. (1987). Methane emission from natural wetlands: global distribution, area, and environmental characteristics of sources. *Global Biogeochemical Cycles, 1(1)*, 61-86. https://doi.org/10.1029/GB001i001p00061

Mcdonald, M. E. (1955). Cause and effects of a die-off of emergent vegetation. *The Journal of Wildlife Management, 19(1)*, 24-35.

McFeeters, S. K. (1996). The use of the normalized difference water index (NDWI) in the delineation of open water features. *International Journal of Remote Sensing*, *17*(7), 1425–1432. https://doi.org/10.1080/01431169608948714

McLeod, E., Chmura, G. L., Bouillon, S., Salm, R., Björk, M., Duarte, C. M., Lovelock, C. E., Schlesinger, W. H., & Silliman, B. R. (2011). A blueprint for blue carbon: Toward an improved understanding of the role of vegetated coastal habitats in sequestering CO_2. *Frontiers in Ecology and the Environment, 9(10)*, 552-560. https://doi.org/10.1890/110004

Moody, A., & Johnson, D. M. (2001). Land-surface phenologies from AVHRR using the discrete fourier transform. *Remote Sensing of Environment*, *75*, 305-323. https://doi.org/10.1016/S0034-4257(00)00175-9

Neubauer. S. C. (2008). Contributions of mineral and organic components to tidal freshwater marsh accretion. *Estuarine, Coastal and Shelf Science, 78*, 78-88. https://doi.org/10.1016/j.ecss.2007.11.011

Olsson, L. and Eklundh, L. (1994). Fourier Series for analysis of temporal sequences of satellite sensor imagery. *International Journal of Remote Sensing 15:* 3735-3741. https://doi.org/10.1080/01431169408954355

Omernik, J. M., Griffith, G. E., Hughes, R. M., Glover, J. B., Weber, M. H., & Weber, M. H. (2017). How misapplication of the Hydrologic Unit Framework diminishes the meaning of watersheds. *Environmental Management*, *60*(1), 1-11. https://doi.org/10.1007/s00267-017-0854-z

Ozesmi, S. L. and Bauer, M. E. (2002). Satellite remote sensing of wetlands. *Wetlands Ecology and Management, 10*: 381-402. https://doi.org/10.1023/A:1020908432489

Pellegrin, D., & Hauber, D. P. (1999). Isozyme variation among populations of the clonal species, *Phragmites australis* (Cav.) Trin. ex Steudel. *Aquatic Botany*, *63*(3-4), 241–259. https://doi.org/10.1016/S0304-3770(98)00120-X

Pettorelli, N., Vik, J. O., Mysterud, A., Gaillard, J. M., Tucker, C. J., Stenseth, N. C. (2005). Using the satellite-derived NDVI to assess ecological responses to environmental change. *TRENDS in Ecology and Evolution, 20(9)*, 503-510. https://doi.org/10.1016/j.tree.2005.05.011

Plut, K., Paul, J., Ciotir, C., Major, M., & Freeland, J. R. (2011). Origin of non-native *Phragmites australis* in North America, a common wetland invader. *Fundamental and Applied Limnology*, *179*(2), 121-129. https://doi.org/10.1127/1863-9135/2011/0179-0121

Reed, B. C., Brown, J. F., VanderZee, D., Loveland, T. R., Merchant, J. W., and Ohlen, D. O. (1994). Measuring phenological variability from satellite imagery. *Journal of Vegetation Science, 5(5):* 703-714. https://doi.org/10.2307/3235884

Rodriguez-Galiano, V. F., Ghimire, B., Rogan, J., Chica-Olmo, M., & Rigol-Sanchez, J. P. (2012). An assessment of the effectiveness of a random forest classifier for land-cover classification. *ISPRS Journal of Photogrammetry and Remote Sensing*, *67*, 93-104. https://doi.org/10.1016/j.isprsjprs.2011.11.002

Rooth, J E, & Stevenson, J. C. (2000). Sediment deposition patterns in Phragmites australis communities: Implications for coastal areas threatened by rising sea-level. *Wetlands Ecology and Management, 8*, 173-183. https://doi.org/10.1023/A:1008444502859

Rooth, Jill E, Stevenson, J. C., & Cornwell, J. C. (2003). Increased Sediment Accretion Rates Following Invasion by Phragmites australis : The Role of Litter. *Estuaries*, *26*(2B), 475–483. https://www.jstor.org/stable/1353362

Roseau Cane Die-Off: Distribution Map. (2019). LSU Ag Center. https://www.lsuagcenter.com/topics/environment/invasive species/roseau cane die-off/distribution map

Roy, D. P., & Yan, L. (2020). Robust Landsat-based crop time series modelling. *Remote Sensing of Environment*, *238*, 110810. https://doi.org/10.1016/j.rse.2018.06.038

Ruppert, D. (2002). Selecting the number of knots for penalized splines. *Journal of Computational and Graphical Statistics*, *11*(4), 735–757. https://doi.org/10.1198/106186002853

Russell, R. J. (1967). *River plains and sea coasts*. University of California Press.

Saltonstall, K. (2002). Cryptic invasion by a non-native genotype of the common reed, *Phragmites australis*, into North America. *Proceedings of the National Academy of Sciences, 99(4)*, 2445-2449. https://doi.org/10.1073/pnas.032477999

Sasser, C.E., Visser, J.M., Mouton, E., Linscombe, J., and Hartley, S.B. (2014). Vegetation types in coastal Louisiana in 2013: U.S. Geological Survey Scientific Investigations Map 3290, 1 sheet, scale 1:550,000

Scott, J. A., Shields, O., & Ellis, S. L. (1977). Distribution and biology of Pleistocene relict: *Ochlodes yuma* (*Hesperiidae*). *Journal of the Lepidoptehists' Society*, *31*(1), 17–22.

Snedden, G. A. (2019). Patterning emergent marsh vegetation assemblages in coastal Louisiana, USA, with unsupervised artificial neural networks. *Applied Vegetation Science*, *22*, 213–229. https://doi.org/10.1111/avsc.12425

Suir, G. M., Saltus, C. L., & Reif, M. K. (2018). *Geospatial Assessments of Phragmites australis Die-off in South Louisiana: Preliminary Findings*.

Temmerman, S., Moonen, P., Schoelynck, J., Govers, G., & Bouma, T. J. (2012). Impact of vegetation die-off on spatial flow patterns over a tidal marsh. *Geophysical Research Letters*, *39*(3). https://doi.org/10.1029/2011GL050502

Townshend, J. R. G., Goff, T. E., & Tucker, C. J. (1985). Multitemporal dimensionality of images of normalized difference vegetation index at continental scales. *IEEE Transactions on Geoscience and Remote Sensing*, *GE-23*(6), 888–895. https://doi.org/10.1109/TGRS.1985.289474

Trautmann, F. (1984). New Orleans, the Mississippi, and the Delta through a German's Eyes: The Travels of Emil Deckert, 1885-1886. *Louisiana History: The Journal of the Louisiana Historical Association*, 25(1): 79-98. https://www.jstor.org/stable/4232330

Tucker, C. J. (1979). Red and photographic infrared linear combinations for monitoring vegetation. *Remote Sensing of Environment*, *8*, 127–150. https://doi.org/10.1016/0034-4257(79)90013-0

U.S. Geological Survey (USGS), & U.S. Department of Agriculture Natural Resources Conservation Service (USDA-NRCS). (2013). Federal standards and procedures for the national Watershed Boundary Dataset (WBD)(4 ed). In *U.S. Geological Survey Techniques and Methods 11–A3* (p. 63).

Uddin, M. N., Caridi, D., & Robinson, R. W. (2012). Phytotoxic evaluation of *Phragmites australis*: An investigation of aqueous extracts of different organs. *Marine and Freshwater Research*, *63*, 777–787. https://doi.org/10.1071/MF12071

Uddin, M. N., & Robinson, R. W. (2017). Changes associated with *Phragmites australis* invasion in plant community and soil properties: A study on three invaded communities in a wetland, Victoria, Australia. *Limnologica*, *66*, 24–30. https://doi.org/10.1016/j.limno.2017.07.006

USACE. (2018). *Mississippi River Ship Channel, Gulf to Baton Rouge, LA: Integrated General Reevaluation Report and Supplemental Environmental Impact Statement*. U.S. Army Corps of Engineers Mississippi Valley Division.

van der Putten, W. H. (1997). Aquatic botany die-back of *Phragmites australis* in European wetlands: An overview of the European Research Programme on Reed Die-back and Progression (1993-1994). *Aquatic Botany*, *59(3-4)*, 263–275.

Van Dijk, A., Callis, S. L., Sakamoto, C. M., and Decker, W. L. (1987). Smoothing vegetation index profiles: an alternative method for reducing radiometric disturbance in NOAA/AVHRR data. *Photogrammetric Engineering and Remote Sensing, 53(8):* 1059-1067.

Vermaat, J. E., Bos, B., & Van Der Burg, P. (2016). Why do reed beds decline and fail to re-establish? A case study of Dutch peat lakes. *Freshwater Biology*, *61*(9), 1580–1589. https://doi.org/10.1111/fwb.12801

Visser, J. M., Sasser, C. E., Chabreck, R. H., & Linscombe, R. G. (1998). Marsh vegetation types of the Mississippi River Deltaic Plain. *Estuaries*, *21*(4B), 818–828. https://doi.org/10.2307/1353283

Visser, J. M., Duke-Sylvester, S. M., Carter, J., and Broussard, W. P. (2013). A Computer Model to Forecast Wetland Vegetation Changes Resulting from Restoration and Protection in Coastal Louisiana. *Journal of Coastal Research, 67(sp1):* 51-59. https://doi.org/10.2112/SI_67_4

Wells, J.T. & Coleman, J. M. (1987). Wetland loss and the subdelta life cycle. *Estuarine, Coastal and Shelf Science*, 25, 111-125.

Xu, H. (2006). Modification of normalised difference water index (NDWI) to enhance open water features in remotely sensed imagery. *International Journal of Remote Sensing*, *27*(14), 3025–3033. https://doi.org/10.1080/01431160600589179

Zhang, X., Friedl, M. A., Schaaf, C. B., Strahler, A. H., Hodges, J. C. F., Gao, F., Reed, B. C., and Huete, A. (2003). Monitoring vegetation phenology using MODIS. *Remote Sensing of Environment, 84(3):* 471-475. https://doi.org/10.1016/S0034-4257(02)00135-9

Zhang, C., Denka, S., & Mishra, D. R. (2018). Mapping freshwater marsh species in the wetlands of Lake Okeechobee using very high-resolution aerial photography and lidar data. *International Journal of Remote Sensing. 39(17)*. 5600-5618. https://doi.org/10.1080/01431161.2018.1455242

Zhu, Z. (2017). Change detection using landsat time series: A review of frequencies, preprocessing, algorithms, and applications. *ISPRS Journal of Photogrammetry and Remote Sensing*, *130*, 370–384. https://doi.org/10.1016/j.isprsjprs.2017.06.013

Zhu, Z., & Woodcock, C. E. (2012). Object-based cloud and cloud shadow detection in Landsat imagery. *Remote Sensing of Environment*, *118*, 83–94. https://doi.org/10.1016/j.rse.2011.10.028

VITA

Aimee Margaret Beaudette, born in Canton, New York, received a dual Bachelor of Science degree in environmental science and biology from Rensselaer Polytechnic Institute in Troy, NY. After receiving her diploma in 2015, she worked as a high school biology and chemistry teacher at a private boarding school. Three years of teaching led Aimee back into academia to pursue her Master of Science degree in Renewable Natural Resources, which she plans to receive August 2020. Aimee is interested in working in the nonprofit or government sectors on the conservation of wetland habitats. Upon completion of her master's degree, she will begin work in the field of conservation with plans to constantly grow and learn from her experiences.